The decay of stably stratified grid turbulence in a viscosity-affected stratified flow regime

Tomoaki Watanabe[1]† and Yulin Zheng[2] and Koji Nagata[2]

[1]Education and Research Center for Flight Engineering, Nagoya University, Furo-cho, Chikusa, Nagoya 464-8603, Japan

[2]Department of Aerospace Engineering, Nagoya University, Nagoya 464-8603, Japan

(Received xx; revised xx; accepted xx)

The decay of stably stratified turbulence generated by a towed rake of vertical plates is investigated by direct numerical simulations (DNS) of temporally evolving grid turbulence in a linearly stratified fluid. The Reynolds number $Re_M = U_0 M/\nu$ is 5000 or 10000 while the Froude number $Fr_M = U_0/MN$ is between 0.1 and 6 (U_0: towing speed; M: mesh size; ν: kinematic viscosity; N: Brunt-Väisälä frequency). The DNS results are compared with the theory of stably stratified axisymmetric Saffman turbulence. Here, the theory is extended to a viscosity-affected stratified flow regime with low buoyancy Reynolds number Re_b, and power laws are derived for the temporal variations of the horizontal velocity scale (U_H) and the horizontal and vertical integral length scales (L_H and L_V). Temporal grid turbulence initialized with the mean velocity deficit of wakes exhibits a k^2 energy spectrum at a low-wavenumber range and invariance of $U_H^2 L_H^2 L_V$, which are the signatures of axisymmetric Saffman turbulence. The decay of various quantities follows the power laws predicted for low-Re_b Saffman turbulence when Fr_M is sufficiently small. However, the decay of U_H^2 at $Fr_M = 6$ is no longer expressed by a power law with a constant exponent. This behaviour is related to the scaling of kinetic energy dissipation rate ε: $\alpha = \varepsilon/(U_H^3/L_H)$ is constant during the decay for $Fr_M \leqslant 1$ while it varies with time for $Fr_M = 6$. We also examine the experimental data of towed-grid experiments by Praud et al. (*J. Fluid Mech.*, vol. 522, 2005, pp. 1-33), which is shown to agree with the theory of low-Re_b Saffman turbulence.

1. Introduction

Homogeneous isotropic turbulence is one of the most fundamental problems considered in turbulence research. The assumption of statistical homogeneity and isotropy simplifies the problem and allows the development of statistical theories. Turbulence far from a wall freely decays with time in the absence of an external force that injects energy into the flow. The theories for the decay of homogeneous isotropic turbulence were developed for the evolution of large-scale motions (Davidson 2004). Two types of isotropic turbulence are widely considered in turbulence theories: one is Saffman turbulence, whose three-dimensional energy spectrum is $E(k \to 0) \sim k^2$ (Saffman 1967), where k is a wavenumber; the other is Batchelor turbulence with $E(k \to 0) \sim k^4$ (Batchelor 1953; Batchelor & Proudman 1956). Saffman turbulence and Batchelor turbulence have integral invariants,

† Email address for correspondence: watanabe.tomoaki@c.nagoya-u.jp

which do not change during the decay. These invariants are related to the conservation of linear momentum for Saffman turbulence and that of angular momentum for Batchelor turbulence. The invariant properties provide the constraint for root-mean-squared (rms) velocity fluctuations U and a longitudinal integral length scale L during the decay, that is $U^2L^3 = \text{Const.}$ for Saffman turbulence and $U^2L^5 = \text{Const.}$ for Batchelor turbulence. The invariant properties suggest that the turbulent kinetic energy $3U^2/2$ decays as $U^2 \sim t^{-6/5}$ for Saffman turbulence and $U^2 \sim t^{-10/7}$ for Batchelor turbulence when the Reynolds number is large enough for the non-dimensional kinetic energy dissipation rate $C_\varepsilon = \varepsilon/(U^3/L)$ to be constant, where ε is the kinetic energy dissipation rate.

These theories of decaying homogeneous isotropic turbulence have been assessed with experimental facilities of homogeneous isotropic turbulence. Nearly homogeneous isotropic turbulence is generated in wind tunnels by installing a grid at the entrance of test sections (Simmonsr & Salter 1934; Comte-Bellot & Corrsin 1966; Uberoi & Wallis 1967). Once turbulence is generated by the grid, it decays in the streamwise direction as the turbulence is advected by the mean flow. The theories for Saffman turbulence and Batchelor turbulence predict how turbulence evolves at large scales when the energy spectrum is given by $E(k) \sim k^2$ or k^4. In realistic situations, turbulence is generated from laminar flows, which do not have the energy spectrum of turbulence. Therefore, the energy spectrum with $E(k) \sim k^2$ or k^4 is formed when turbulence is generated. The theories do not clarify under what conditions turbulence with $E(k) \sim k^2$ or k^4 develops from a laminar flow. For this reason, it is not straightforward to determine whether grid turbulence belongs to Saffman turbulence, Batchelor turbulence or others. Experiments of grid turbulence often compare the evolutions of statistics with the theories of Saffman turbulence and Batchelor turbulence. In the theories, U^2L^3 and U^2L^5 are invariants of Saffman turbulence and Batchelor turbulence, respectively. Wind-tunnel experiments have confirmed that U^2L^3 hardly varies during the decay, indicating that the grid turbulence behaves similarly to Saffman turbulence (Krogstad & Davidson 2010; Kitamura *et al.* 2014). The decay exponent of the turbulent kinetic energy is generally close to that of Saffman turbulence (Krogstad & Davidson 2010; Kitamura *et al.* 2014; Sinhuber *et al.* 2015; also see the papers cited in these studies). However, a discrepancy of the decay exponent from Saffman turbulence is also pointed out as the values of the exponent vary depending on experiments (Antonia *et al.* 2013; Djenidi *et al.* 2015). The decay exponent is sensitive to the behaviour of two-point correlations at a large separation distance. Variations of the decay exponent can be caused by the effects of the finite size of wind tunnels because the walls can affect the long-range correlation of turbulence. An error in estimating the decay exponent may arise from the finite number of measurement points. In addition, the decay exponent is also sensitive to the turbulent Reynolds number Re_λ when Re_λ is not sufficiently large. The decay exponent may not be constant during the decay in previous experiments with moderate Re_λ (Djenidi *et al.* 2015). These issues in experiments of grid turbulence cause difficulty in concluding whether or not grid turbulence is Saffman turbulence.

Turbulence with stable density stratification is a common phenomenon observed in the environment, e.g. the atmospheric boundary layer (Mahrt 1999) and the ocean mixing layer (Thorpe 1978). The stable stratification can significantly alter the dynamics of turbulence because the stratification supports the propagation of internal gravity waves and suppresses vertical turbulent motions. Therefore, stably stratified turbulence has been extensively investigated by theories, laboratory experiments and numerical simulations for many years. As nearly homogeneous isotropic turbulence generated by a grid is useful to reveal the basic physics of turbulence, experiments have been conducted for grid turbulence in a stably stratified fluid. These experiments generate turbulence

with a grid installed to wind tunnels or water channels (Itsweire *et al.* 1986; Yoon & Warhaft 1990; Lienhard & van Atta 1990; Huq & Britter 1995; Komori & Nagata 1996) and a grid towed in a density-stratified water tank (Britter *et al.* 1983; Yap & Van Atta 1993; Liu 1995; Fincham *et al.* 1996; Rehmann & Koseff 2004; Praud *et al.* 2005; Espa *et al.* 2018). Grid turbulence generated in a freestream of wind tunnels decays with the distance x from the grid. On the other hand, turbulence in towed-grid experiments decays with time t. However, these experiments can be compared by converting the distance x in wind-tunnel experiments to time as $t = x/U_0$ with the mean velocity U_0.

The effects of stable stratification on the decay rate of turbulent kinetic energy have been reported in these experimental studies. However, the reported results are not conclusive: some experiments found that the decay rate is increased by the stratification while others found different effects, e.g. slower decay or no stratification influence on the decay rate. Wind-tunnel experiments of non-stratified grid turbulence have confirmed that the decay can be divided into three regimes: an initial, non-equilibrium decay period, where C_ε increases as turbulence decays; an equilibrium decay period with constant C_ε; a final period of decay. The decay exponent close to Saffman turbulence was obtained for the equilibrium decay period in wind-tunnel experiments. When the turbulent Reynolds number is low, C_ε increases toward the final period of decay. The decay of U^2 is described by $dU^2/dt = -C_\varepsilon(U^3/L)$, which is used together with $U^2L^3 = \text{Const.}$ or $U^2L^5 = \text{Const.}$ to derive $U^2 \sim t^n$. The decay exponents of Saffman turbulence and Batchelor turbulence are obtained with the assumption of constant C_ε. If C_ε increases with time, n becomes larger than those derived for constant C_ε. Indeed, the decay exponent obtained for the near-grid region is larger than 1.2 of Saffman turbulence (Komori *et al.* 1993; Krogstad & Davidson 2012). Some experiments of stably stratified grid turbulence conducted the measurement in the near-grid region with small t, which may be inadequate for comparison with other studies. Another issue that may affect the discussion of the decay exponent is the virtual origin of the decay law. The decay of grid turbulence is more accurately expressed as $U^2 \sim (t - t_0)^n$ with the virtual origin t_0, whose estimation from experimental data is crucial to determine n. For non-stratified grid turbulence, various methods have been proposed to determine both n and t_0 (Mohamed & LaRue 1990; Lavoie *et al.* 2007; Krogstad & Davidson 2010; Valente & Vassilicos 2011). However, the assumption of $t_0 = 0$ is widely used in studies of stably stratified grid turbulence even though there is no reason for the virtual origin to be zero (Liu 1995; Praud *et al.* 2005).

Important theoretical analyses of decaying homogeneous turbulence in a linearly stratified fluid were presented in Davidson (2009, 2010) based on the theories for axisymmetric Saffman and Batchelor turbulence. One of the important non-dimensional parameters in the decay of stratified homogeneous turbulence is the buoyancy Reynolds number $Re_b = \varepsilon/N^2\nu$, where N is a Brunt-Väisälä frequency and ν is a kinematic viscosity. As discussed in §2 with more details, the constraints similar to $U^2L^3 = \text{Const.}$ and $U^2L^5 = \text{Const.}$ were used to derive the decay laws of strongly stratified homogeneous turbulence at high Re_b. However, experiments of stably stratified grid turbulence failed to reproduce the decay laws of the theories. Most experiments of stratified grid turbulence have been conducted for low Reynolds numbers, and it is plausible that the assumption used to derive the decay laws at high Re_b was not valid in the experiments. Interesting findings related to the Re_b effects on the decay were reported by de Bruyn Kops & Riley (2019), where direct numerical simulations (DNS) were conducted for decaying, stably stratified homogeneous turbulence initialized with isotropic turbulence with the Saffman spectrum. The decay of turbulence is consistent with the theory in Davidson (2010) when Re_b is sufficiently large. However, they observed the deviation from the theory once Re_b becomes very small after the turbulence decays sufficiently.

This study aims to investigate the decay of grid turbulence in a stably stratified fluid at a low Re_b regime, which was not covered by the theories by Davidson (2009, 2010) but was extensively investigated in experiments of grid turbulence. The theories of decaying homogeneous turbulence in a linearly stratified fluid (Davidson 2009, 2010) are extended to the low Re_b regime and are utilized to derive the decay laws of horizontal kinetic energy, horizontal and vertical integral scales, kinetic energy dissipation rate, and potential energy. Furthermore, DNS is conducted for a numerical model of stably stratified grid turbulence generated by a rake of vertical flat plates, which was experimentally studied by Fincham *et al.* (1996) and Praud *et al.* (2005). It is natural to assume that the production process of turbulence determines the shape of $E(k)$ although how Saffman or Batchelor turbulence is generated is not explained by the theories. In laboratory experiments, the production process of grid turbulence includes many complicated phenomena, such as the production of turbulent kinetic energy due to mean shear (Nagata *et al.* 2013; Valente & Vassilicos 2015), vortex shedding from each bar (Melina *et al.* 2016) and the boundary layer separation on the grid surface (Sarpkaya 2006). Therefore, laboratory experiments may not be enough to reveal which part of the production process of grid turbulence is essential to generate Saffman turbulence or Batchelor turbulence. Because turbulence is generally a complicated phenomenon that is difficult to interpret, fundamental studies of turbulence often consider simplified problems, such as isotropic turbulence and temporally evolving shear flows (Pope 2000). Even though these ideal and simplified models of turbulence may not be realized in laboratories in a precise sense, their analyses can highlight essential aspects of turbulent flows. In this spirit, this study considers a temporally evolving grid turbulence (Watanabe & Nagata 2018). The temporally evolving grid turbulence is initialized with a velocity field that approximates the mean velocity deficit of the wakes of bars or plates. The production of turbulence occurs due to the mean shear while other phenomena related to the grid object, such as vortex shedding, are excluded from the simulation. It will be shown that a stably stratified flow initialized in this way develops into turbulence with the signatures of axisymmetric Saffman turbulence.

The remainder of this paper is organized as follows. The theories for Saffman turbulence and Batchelor turbulence at low Re_b in a stably stratifie fluid are presented in §2. The numerical methodology of temporally evolving grid turbulence is described in §3. The DNS results are shown in §4, where the evolution of grid turbulence is compared with the theories in §2. In §5, the experimental data in the existing literature is compared with the theories. The results suggest that turbulence generated by a vertical grid in a stably stratified fluid behaves similarly to axisymmetric Saffman turbulence. Finally, the paper is summarized in §6.

2. Decay of stably stratified homogeneous turbulence

We consider a Boussinesq fluid, where the effects of density variations appear only as a buoyancy force. It is also assumed that a density field is given by $\overline{\rho}(z) + \rho(x, y, z, t)$ with an unperturbed density distribution $\overline{\rho}$ and a density perturbation ρ, where the vertical gradient $d\overline{\rho}/dz$ is uniform. The governing equations are the Navier–Stokes equations with

the Boussinesq approximation, which are written as

$$\frac{\partial u_j}{\partial x_j} = 0, \tag{2.1}$$

$$\frac{\partial u_i}{\partial t} + \frac{\partial u_i u_j}{\partial x_j} = -\frac{1}{\rho_0}\frac{\partial p}{\partial x_i} + \nu\frac{\partial^2 u_i}{\partial x_j \partial x_j} - \frac{g\rho}{\rho_0}\delta_{i3}, \tag{2.2}$$

$$\frac{\partial \rho}{\partial t} + \frac{\partial \rho u_j}{\partial x_j} + w\frac{d\overline{\rho}}{dz} = D\frac{\partial^2 \rho}{\partial x_j \partial x_j}, \tag{2.3}$$

where u_i is the i-th component of the velocity vector, p is the pressure, ρ_0 is the constant mean density, D is the diffusivity coefficient for density, δ_{ij} is the Kronecker's delta and g is the gravitational acceralation. The subscripts $i = 1, 2$ and 3 denote x, y and z directions, respectively, and the velocity components in these directions are denoted by u, v and w.

The decay of freely-evolving, stably stratified homogeneous turbulence is considered in this study. Here, we introduce several important parameters of the flow. An average of a variable f is defined as a volume average $\langle f \rangle_V(t) = V^{-1}\iiint f(x, y, z, t)dxdydz$, where V is the integral volume. A velocity scale of large-scale horizontal motions is defined as $U_H = \langle u^2 \rangle_V^{1/2}$. The integral scales in the horizontal and vertical directions are denoted by L_H and L_V, respectively, and are defined with the auto-correlation functions of horizontal velocity as

$$L_H(t) = \frac{1}{\langle u^2 \rangle_V}\int \langle u(x, y, z, t)u(x + r, y, z, t)\rangle_V dr, \tag{2.4}$$

$$L_V(t) = \frac{1}{\langle u^2 \rangle_V}\int \langle u(x, y, z, t)u(x, y, z + r, t)\rangle_V dr. \tag{2.5}$$

For the linear density profile of $\overline{\rho}$, the mean potential energy is defined as $E_P = \langle b^2 \rangle_V/2$ with the buoyancy $b = \rho g/\rho_0 N$. The governing equations for kinetic energy $k_T = \langle u_i u_i \rangle_V/2$ and potential energy are given by

$$\frac{\partial k_T}{\partial t} = -\langle 2\nu S_{ij} S_{ij} \rangle_V - \frac{g}{\rho_0}\langle w\rho \rangle_V, \tag{2.6}$$

$$\frac{\partial E_P}{\partial t} = -D\langle \nabla b \cdot \nabla b \rangle_V + \frac{g}{\rho_0}\langle w\rho \rangle_V. \tag{2.7}$$

The second terms on the right-hand side of these equations are the buoyancy flux and represent the energy exchange between kinetic energy and potential energy. The dissipation rates of k_T and E_P are given by $\varepsilon = \langle 2\nu S_{ij} S_{ij} \rangle_V$ and $\varepsilon_P = D\langle \nabla b \cdot \nabla b \rangle_V$, where $S_{ij} = (\partial u_i/\partial x_j + \partial u_j/\partial x_i)/2$ is a rate-of-strain tensor.

The Kolmogorov scale represents the smallest scale of turbulent motions and is defined by $\eta = (\nu^3/\varepsilon)^{1/4}$. It is often considered that the stratification significantly suppresses vertical turbulent motions at scales greater than the Ozmidov scale, which is defined as $L_O = (\varepsilon/N^3)^{1/2}$ with $N = \sqrt{-(g/\rho_0)d\overline{\rho}/dz}$. The relative strength of stratification is evaluated with the horizontal Froude number $Fr_H = U_H/L_H N$, which is defined as the ratio between the buoyancy period $1/N$ and the time scale of large-scale horizontal motions L_H/U_H. The buoyancy Reynolds number is defined with the length scale ratio between L_O and η as

$$Re_b = \left(\frac{L_O}{\eta}\right)^{4/3} = \frac{\varepsilon}{N^2\nu}. \tag{2.8}$$

Turbulent motions at scales below L_O is not significantly suppressed by the stable

stratification, and there is a range of scales with small-scale turbulent fluctuations if $Re_b \gg \mathcal{O}(10^0)$. On the other hand, the small-scale turbulent motions are also inhibited by the stratification for $Re_b \leqslant \mathcal{O}(10^0)$. The Reynolds number of large-scale horizontal motions can be defined as $Re_H = U_H L_H/\nu$. It should be noted that one can relate Re_b to Re_H and Fr_H as $Re_b \sim Re_H Fr_H^2$ with the dissipation scaling $\varepsilon \sim U_H^3/L_H$, which is often assumed for stratified turbulence (Riley & de Bruyn Kops 2003; Brethouwer *et al.* 2007).

2.1. *Decay laws of Saffman and Batchelor turbulence at high Re_b*

First, we briefly review the decay laws derived in Davidson (2009, 2010) for Saffman and Batchelor turbulence in a stably stratified fluid at high Re_b. Davidson (2010) adapted the theory of axisymmetric Saffman turbulence to freely evolving, stably stratified homogeneous turbulence and obtained

$$U_H^2 L_H^2 L_V = \text{Const.}, \tag{2.9}$$

which is required for the Saffman-like invariant to be constant when the large scales evolve in a self-similar manner. Similarly, the following constraint was derived for axisymmetric Batchelor turbulence in a stably stratified fluid (Davidson 2009):

$$U_H^2 L_H^4 L_V = \text{Const.}, \tag{2.10}$$

which is also required for the Loitsyansky-like integral to be constant.

Equations (2.9) and (2.10) are satisfied during the decay and are directly related to the decay law of stably stratified homogeneous turbulence. The cases with high $Re_b \sim Re_H Fr_H^2$ with low Fr_H and high Re_H were considered in Davidson (2009, 2010), where the following assumptions were made:

$$\frac{dU_H^2}{dt} = -\alpha \frac{U_H^3}{L_H}, \tag{2.11}$$

$$\frac{U_H}{N L_V} = C, \tag{2.12}$$

where α and C are dimensionless constants of order one. The first assumption concerns the non-dimensional kinetic energy dissipation rate $\alpha = \varepsilon L_H/U_H^3$ while the second one can be derived from the balance between inertial and buoyancy forces for $Re_b \sim Re_H Fr_H^2 \gg 1$ (Lindborg 2006). Equations (2.11) and (2.12) combined with (2.9) yield the following power laws for axisymmetric Saffman turbulence in a stably stratified fluid (Davidson 2010):

$$U_H^2 \sim t^{-4/5},\ L_H \sim t^{3/5},\ L_V \sim t^{-2/5},\ \varepsilon \sim t^{-9/5}. \tag{2.13}$$

On the other hand, (2.10), (2.11) and (2.12) yield the following decay laws for Batchelor turbulence (Davidson 2009):

$$U_H^2 \sim t^{-8/7},\ L_H \sim t^{3/7},\ L_V \sim t^{-4/7},\ \varepsilon \sim t^{-15/7}. \tag{2.14}$$

The decay of U_H^2 is slower than non-stratified isotropic turbulence, for which $U^2 \sim t^{-6/5}$ in Saffman turbulence and $U^2 \sim t^{-10/7}$ in Batchelor turbulence. Furthermore, the integral scale increases as non-stratified isotropic turbulence decays while L_V decreases with time in (2.13) and (2.14).

In addition to the above power laws obtained by Davidson (2009, 2010), we can also derive the decay laws of potential energy for Saffman and Batchelor turbulence. From the balance between the pressure gradient and the buoyancy term in the governing equation

of w, one can assume that the density perturbation ρ is scaled by $U_H^2\rho_0/gL_V$ (Godoy-Diana *et al.* 2004), or equivalently

$$E_P \sim U_H^4/N^2L_V^2. \tag{2.15}$$

This scaling combined with (2.13) or (2.14) yields the following power laws for the decay of E_P at high Re_b:

$$E_P \sim t^{-4/5} \quad \text{for high-}Re_b\text{ Saffman turbulence,} \tag{2.16}$$

$$E_P \sim t^{-8/7} \quad \text{for high-}Re_b\text{ Batchelor turbulence.} \tag{2.17}$$

The decay exponents of E_P are the same as those of U_H^2. The kinetic energy k_T is dominated by the horizontal velocity in strongly stratified turbulence, and therefore the ratio E_P/k_T is constant during the decay.

2.2. *Alternative decay laws for low Re_b*

The above decay laws derived for high Re_b have not been verified in stably stratified grid turbulence most probably because the Reynolds number is not sufficiently high in experiments. For example, Praud *et al.* (2005) found that L_V increases with time in the towed-grid experiments while L_V is expected to decrease for high-Re_b Saffman and Batchelor turbulence. In this section, we derive the decay laws of stably stratified homogeneous turbulence at low Re_b, which should be more relevant to most experimental studies of decaying stratified turbulence. Stratified turbulence at low Re_b is often referred to as the viscosity-affected stratified flow regime (Brethouwer *et al.* 2007). For this regime, Godoy-Diana *et al.* (2004) assumed that the vertical length scale is determined as a result of the balance between the horizontal advection and the vertical diffusion and proposed the relation between L_H and L_V given by $L_V \sim L_H Re_H^{-1/2}$. From the definition of Re_H one can expect the following relation during the decay:

$$L_V \sim \left(\nu\frac{L_H}{U_H}\right)^{1/2}, \tag{2.18}$$

where ν is treated as a constant parameter in each flow. When the kinetic energy dissipation is assumed to be dominated by the vertical gradient of horizontal velocity at low Re_b, the dissipation rate is estimated as $\varepsilon \sim \nu U_H^2/L_V^2$. This relationship can be combined with (2.18) to derive $\varepsilon \sim U_H^3/L_H$, which leads to (2.11) even for low Re_b (Brethouwer *et al.* 2007; Maffioli & Davidson 2016). Then, (2.11) and (2.18) combined with (2.9) yield the following decay laws of Saffman turbulence at low Re_b:

$$U_H^2 \sim t^{-5/4}, \quad L_H \sim t^{3/8}, \quad L_V \sim t^{1/2}, \quad \varepsilon \sim t^{-9/4}. \tag{2.19}$$

For the Batchelor turbulence, the following decay laws are derived with (2.10), (2.11) and (2.18):

$$U_H^2 \sim t^{-3/2}, \quad L_H \sim t^{1/4}, \quad L_V \sim t^{1/2}, \quad \varepsilon \sim t^{-5/2}. \tag{2.20}$$

Here, the decay laws of ε are derived from $\varepsilon = \alpha U_H^3/L_H$ with a constant α.

As also discussed for high Re_b cases, the decay laws of E_P can be derived from $E_P \sim U_H^4/N^2L_V^2$ combined with (2.19) or (2.20). These decay laws can be written as

$$E_P \sim t^{-7/2} \quad \text{for low-}Re_b\text{ Saffman turbulence,} \tag{2.21}$$

$$E_P \sim t^{-4} \quad \text{for low-}Re_b\text{ Batchelor turbulence.} \tag{2.22}$$

In this study, it will be shown that these decay laws for low-Re_b Saffman turbulence prevail in stably stratified grid turbulence at low Froude numbers.

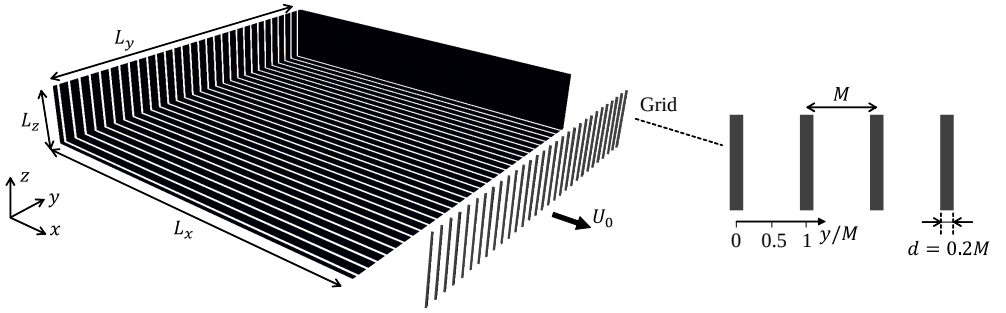

Figure 1: The initial condition of DNS of temporally evolving grid turbulence. White and black regions, shown on the domain boundaries, have the initial mean velocity of $(1 - D/M)U_0$ and $-(D/M)U_0$, respectively. The grid geometry is also shown beside the computational domain. Statistics are calculated between $y/M = 0$ and 1.

3. DNS of temporally evolving stably stratified grid turbulence

3.1. *Temporally evolving stably stratified grid turbulence*

Direct numerical simulations (DNS) are carried out for a numerical model of towed-grid experiments conducted by Praud *et al.* (2005) and Fincham *et al.* (1996). Here, we consider a temporally evolving grid turbulence as an approximation of the grid turbulence generated by a towed grid. Non-stratified, temporally evolving grid turbulence was studied with DNS in Watanabe & Nagata (2018), where the evolutions of various velocity statistics were shown to be quantitatively consistent with wind-tunnel experiments and towed grid experiments without density stratification. The grid considered in the present DNS is a rake of vertical flat plates with a mesh size M (Praud *et al.* 2005). The thickness of each plate D is $0.2M$, which yields a solidity of 0.2. The grid is towed in the horizontal (x) direction at a constant speed U_0 in a stably stratified fluid with a constant $d\overline{\rho}/dz$. Each plate generates a turbulent wake, and the wake interaction results in the formation of grid turbulence.

Simulations of temporally evolving grid turbulence adapt the methodology used to simulate temporally evolving turbulent shear flows, which are also studied as an approximation of spatially evolving counterparts. Temporal simulations of turbulent shear flows use a periodic boundary condition in the streamwise direction, and the flow develops with time instead of the streamwise direction (da Silva & Pereira 2008; Pham *et al.* 2009; Diamessis *et al.* 2011; Gampert *et al.* 2014; Watanabe *et al.* 2015; Kozul *et al.* 2016; Watanabe *et al.* 2018*b*). The temporally evolving grid turbulence is also simulated in a triply periodic box (Watanabe & Nagata 2018). Simulations of temporally evolving wakes are often initialized with a tophat mean velocity profile for which different mean velocity values are applied to the freestream and the wake region behind an object (Zecchetto & da Silva 2021). Then, the shear due to the mean velocity difference results in the development of the turbulent wake. Following the approach used for temporal wakes, the DNS of temporally evolving grid turbulence is initialized with the following velocity and

density profiles (Watanabe & Nagata 2018):

$$u(x,y,z,t=0) = \langle u\rangle(y,t=0) + u'(x,y,z), \tag{3.1}$$

$$v(x,y,z,t=0) = v'(x,y,z), \tag{3.2}$$

$$w(x,y,z,t=0) = w'(x,y,z), \tag{3.3}$$

$$\rho'(x,y,z,t=0) = 0, \tag{3.4}$$

$$\langle u\rangle(y,t=0) = \begin{cases} (1-D/M)U_0 & \text{behind plates} \\ -(D/M)U_0 & \text{otherwise} \end{cases}. \tag{3.5}$$

Here, $\langle f\rangle(y,t) = (1/L_xL_z)\iint f(x,y,z,t)dxdz$ is the average taken on a x-z plane, where (L_x, L_y, L_z) is the computational domain size, while fluctuations are denoted by $f' = f - \langle f\rangle$. Figure 1 shows the initial profile of the mean velocity $\langle u\rangle$. The velocity difference between the two regions is U_0 for (3.5). Here, the mean velocity profile is derived by subtracting $(D/M)U_0$ from U_0 and 0 so that the volume average of u is zero. This enables us to adapt a large time increment at a late time because the instantaneous velocity becomes small with time. Initial velocity perturbations (u', v', w') are obtained by the method that generates spatially-correlated fluctuations from random numbers (Watanabe *et al.* 2019*b*; Hayashi *et al.* 2021; Watanabe & Nagata 2021). The characteristic length scale of (u', v', w') is $0.1M$ and the initial rms velocity fluctuations are $0.005U_0$, which is as small as the background fluctuations in wind-tunnel experiments of grid turbulence (Seoud & Vassilicos 2007; Kitamura *et al.* 2014). The Brunt-Väisälä frequency N is constant and is not varied with time. Therefore, the initial flow field is already stably stratified. This is contrary to some other simulations of decaying turbulence, which imposes stratification after the turbulence freely decays for a short time without the stratification (Diamessis *et al.* 2011; de Bruyn Kops & Riley 2019). Experiments of towed-grid turbulence are prepared by filling a tank with a stratified fluid. Then, the grid is towed in the tank to generate grid turbulence. Wind-tunnel experiments also introduce stable stratification before the flow passes a grid. These situations are better approximated in DNS of temporally evolving grid turbulence by initializing the flow field with a stratified fluid because the generation process of grid turbulence is strongly influenced by stable stratification, as also discussed by Okino & Hanazaki (2019).

Most statistics presented in this paper are calculated as functions of y in the range of $0 \leqslant y/M \leqslant 1$ as shown in figure 1. Here, the grid consists of a large number of vertical plates. The samples in $0 \leqslant y/M \leqslant 1$ are taken from all the plates because the wake of each plate is statistically identical. In grid turbulence, $\langle f\rangle(y,t)$ is different from the volume average $\langle f\rangle_V(t)$ in the near-grid region, which corresponds to an early time of temporally evolving grid turbulence. Once grid turbulence has fully developed, the statistics do not depend on y. Then, $\langle f\rangle(y,t)$ is identical to $\langle f\rangle_V(t)$. The decay laws of grid turbulence are examined with the statistics defined with the x–z average $\langle f\rangle(y,t)$ while the volume average is used for comparison with experimental data.

3.2. *Numerical methods and parameters*

The temporally evolving grid turbulence is simulated with the DNS code that solves (2.1-2.3) with the fractional step method. This code has been used in our previous studies on homogeneous isotropic turbulence and stably stratified turbulent shear layers (Watanabe *et al.* 2018*a*, 2019*a*, 2020). Spatial derivatives are computed with the fully-conservative fourth-order central difference scheme (Morinishi *et al.* 1998). Time is

Table 1: Computational and physical parameters of DNS. The size of the computational domain is (L_x, L_y, L_z), which is represented by $N_x \times N_y \times N_z$ grid points. At time t_H, the production rate of turbulent kinetic energy becomes smaller than 1 % of the dissipation rate as examined in figure 8. The time at which the flow enters a viscosity-affected stratified flow regime is denoted by t_V, which is obtained from figure 9. Time t_V is normalized by the reference time scale of grid turbulence t_r or the buoyancy period $1/N$.

Run	Re_M	Pr	Fr_M	L_x	L_y	L_z	N_x	N_y	N_z	t_H/t_r	t_V/t_r	$t_V N$
R5F04	5000	1	0.4	$30M$	$30M$	$5M$	2916	2916	486	18	17	43
R5F1	5000	1	1	$30M$	$30M$	$5M$	2916	2916	486	25	22	22
R10F01	10000	1	0.1	$30M$	$30M$	$5M$	4374	4374	728	12	8	80
R10F04	10000	1	0.4	$30M$	$30M$	$5M$	4374	4374	728	19	32	80
R10F1	10000	1	1	$30M$	$30M$	$5M$	4374	4374	728	26	45	45
R10F6	10000	1	6	$30M$	$30M$	$5M$	4374	4374	728	33	67	11

advanced with a third-order Runge-Kutta method. The biconjugate gradient stabilized method is used to solve the Poisson equation for pressure.

Table 1 summarizes the computational parameters of DNS. The stably stratified grid turbulence can be characterized by the Reynolds number Re_M, Prandtl number Pr and Froude number Fr_M defined as

$$Re_M = \frac{U_0 M}{\nu},\ Pr = \frac{\nu}{D},\ Fr_M = \frac{U_0}{MN}. \tag{3.6}$$

DNS is performed for five sets of (Re_M, Fr_M) with $Pr = 1$. The simulations are performed until $t/t_r = 250$, where $t_r = M/U_0$ is the characteristic time scale. This normalization t/t_r is useful because the normalized streamwise distance from a grid in wind-tunnel experiments, x/M, is equivalent to t/t_r, where $x/U_0 = t$ is the advection time from the grid to the location x. The domain size with $L_x, L_y > L_z$ is used because the horizontal integral scales are much larger than the vertical scale in stably stratified turbulence. The integral scales increase with time. However, even at the end of simulations, the domain size is larger than 12 times the integral length scales, which is large enough to prevent the confinement effects on the decay of turbulence (Anas *et al.* 2020). The number of the grid points (N_x, N_y, N_z) is determined based on the Kolmogorov scale η. The kinetic energy dissipation rate in grid turbulence is evaluated as $\varepsilon = \nu\langle(\partial u_i'/\partial x_j)^2\rangle$ because the flow is initially inhomogeneous. The grid spacing Δ is uniform in three directions. The Kolmogorov scale becomes the smallest in the production phase of grid turbulence and increases with time as the turbulence decays. The largest value of Δ/η is about 1.6 at $t/t_r \approx 7$, at which the flow is highly inhomogeneous, and Δ/η becomes smaller than 1 when grid turbulence has fully developed. Small-scale fluctuations of turbulence are well resolved with this resolution for the present schemes (Watanabe *et al.* 2018*a*). The time increment Δt is determined with a constant Courant number CFL = 0.3, which is also small enough to capture wave motions with the frequency N.

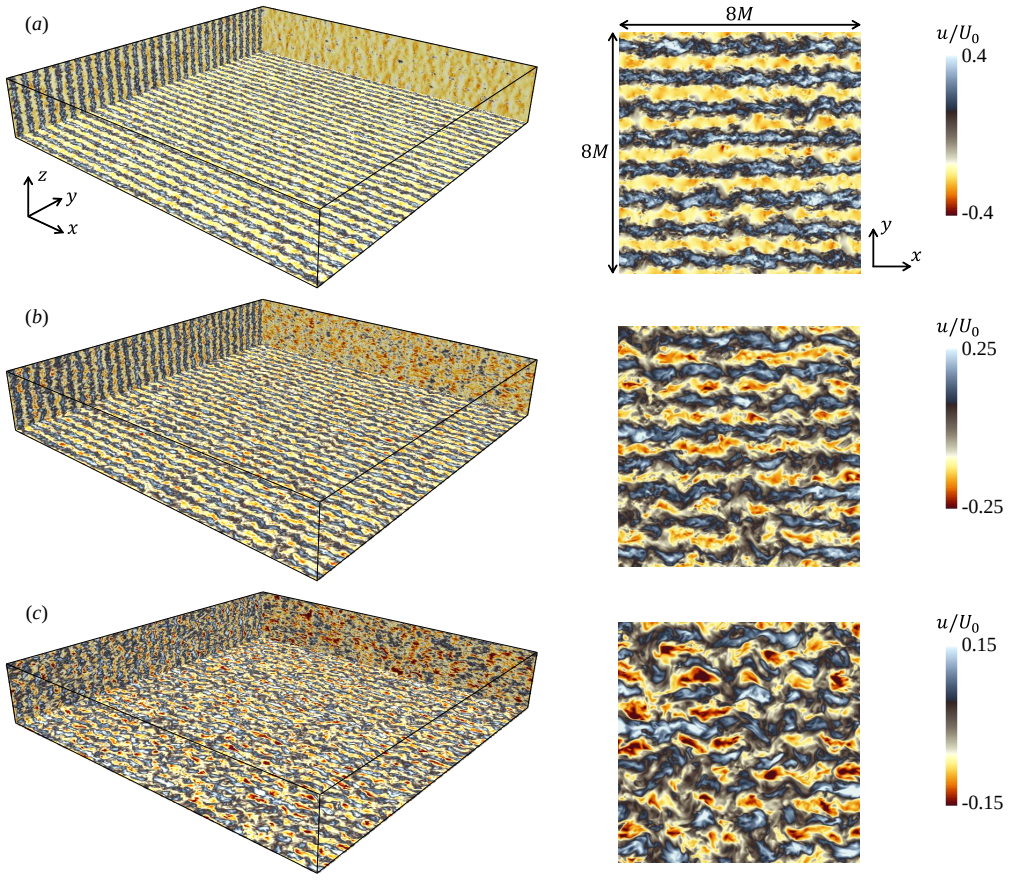

Figure 2: Development of temporally evolving grid turbulence in R10F1 at (*a*) $t/t_r = 5$, (*b*) $t/t_r = 10$ and (*c*) $t/t_r = 15$. The streamwise velocity u is visualized on the boundaries of the computational domain on left panels while two-dimensional contours of u on a x-y plane are shown on right panels.

4. Results and discussion

4.1. *Development of stably stratified grid turbulence*

Figure 2 visualizes the development of grid turbulence in R10F1. The left panels show the colour contour of u on the surfaces of the computational domain while the right panels visualize u on a small part of a x-y plane. At $t/t_r = 5$ in (*a*), the instantaneous velocity profiles are strongly influenced by the wakes of the vertical plates. The wakes develop with time and interact with each other, resulting in the formation of the fully developed grid turbulence. Figure 3 visualizes u on a vertical plane at $t/t_r = 15$ in R10F01 and R10F6. The strongly stable stratification at $Fr_M = 0.1$ causes highly anisotropic velocity fluctuations. However, more isotropic distribution of u is found for $Fr_M = 6$. For both Fr_M, the imprints of the wakes are hardly seen in the velocity profiles, and the grid turbulence has developed by this time.

Figure 4 compares the temporal evolution of volume-averaged horizontal kinetic energy $\langle u^2 + v^2 \rangle_V / 2$ between the DNS and experiments of towed-grid experiments by Praud *et al.* (2005), where the average is taken in the computational domain of DNS or the measurement volume of scanning particle image velocimetry. The experiments were

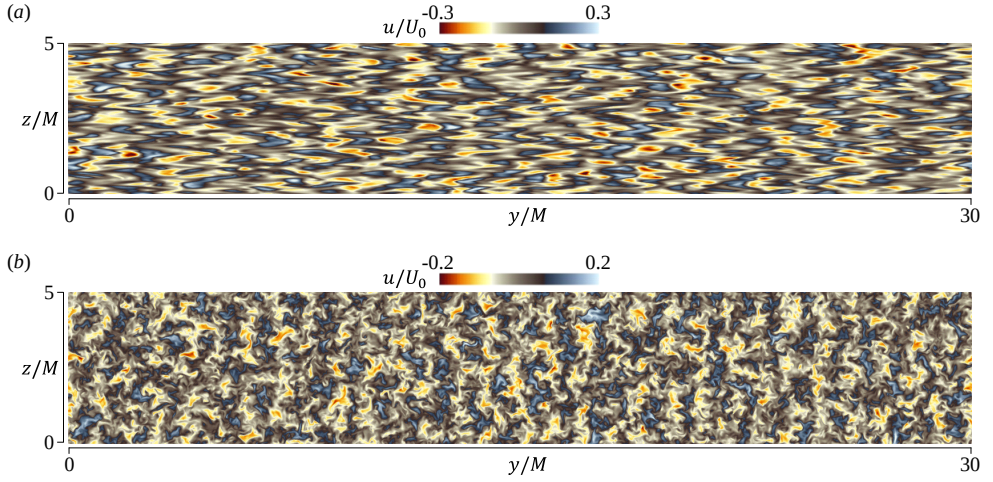

Figure 3: Streamwise velocity profiles on a vertical plane in (a) R10F01 and (b) R10F6 at $t/t_r = 15$.

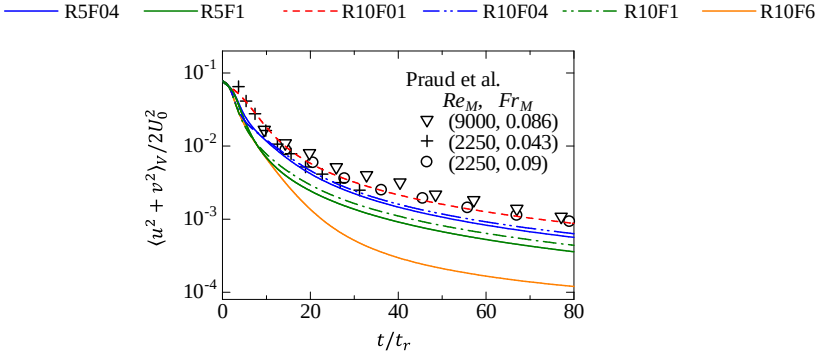

Figure 4: Temporal evolutions of volume-averaged horizontal kinetic energy $\langle u^2+v^2\rangle_V/2$ compared with towed-grid experiments by Praud *et al.* (2005).

conducted in a water tank, where the density stratification was generated with saltwater. Therefore, the Schmidt number was much larger than 1 in the experiments while all DNS consider $Pr = 1$, and this difference may affect the comparison between the DNS and experiments. Figure 4 shows that the horizontal kinetic energy decreases with time. The present DNS with small Fr_M agrees well with the experiments, which were also conducted with $Fr_M \approx 0.1$. The horizontal kinetic energy contains the contribution from both mean and fluctuating velocity components. When the grid turbulence is generated, the kinetic energy in the mean velocity is converted to that of the velocity fluctuations by the production term of turbulent kinetic energy, which is expressed as the product of the Reynolds stress and the mean velocity gradient. The decay of horizontal velocity fluctuations is caused by the viscous dissipation once grid turbulence has fully developed. Although the mean velocity profile given as the initial condition of DNS is only a simple approximation of the flow behind a grid, the initial decay of $\langle u^2+v^2\rangle_V/2$ is in good agreement between the DNS and the experiments. In the DNS, the horizontal kinetic energy tends to be small for large Fr_M while the Re_M dependence is not significant for

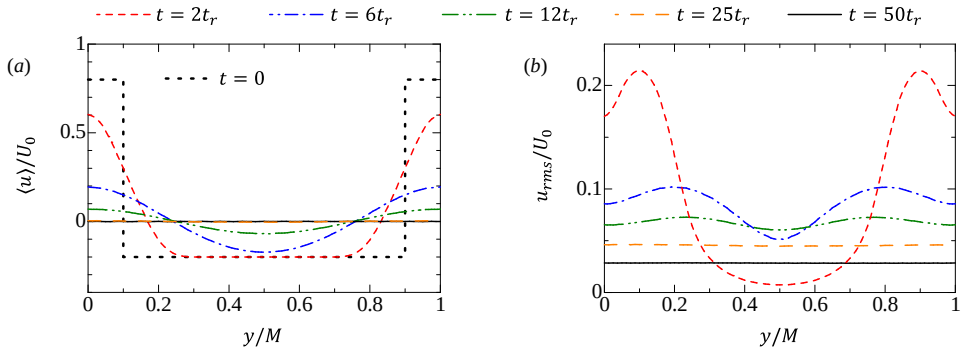

Figure 5: Lateral profiles of (a) mean velocity $\langle u \rangle$ and (b) rms velocity fluctuations u_{rms} in R10F1. The results are taken at five instances of $t/t_r = 2$, 6, 12, 25 and 50.

a fixed value of Fr_M. The energy production by the mean velocity gradient contributes to the growth of the streamwise velocity component of turbulent kinetic energy, which is converted to the other components by the pressure-strain correlation (Pope 2000). This conversion to the vertical component is suppressed in a stably stratified fluid, and a smaller amount of horizontal kinetic energy is converted to the vertical component at lower Fr_M during the production phase of grid turbulence. This stratification effect explains larger $\langle u^2 + v^2 \rangle_V / 2$ for smaller Fr_M.

Figure 5 shows the lateral profiles of mean velocity $\langle u \rangle$ and rms velocity fluctuations $u_{rms} = \langle u'^2 \rangle^{1/2}$. The turbulent wake develops for $0 \leqslant y/M \leqslant 0.1$ and $0.9 \leqslant y/M \leqslant 1$ and the mean velocity difference between the wake and the open region of the grid becomes small with time. The mean velocity profile is homogeneous at $t/t_r = 25$. The velocity fluctuations in the x direction are generated by the mean velocity gradient, which is large at $y/M = 0.1$ and 0.9 at $t/t_r = 2$. Therefore, u_{rms} also reaches peaks at these locations. The wakes spread in the y direction and merge with the adjacent wakes. The profile of u_{rms} also becomes homogeneous at $t/t_r = 25$, and u_{rms} decays with time.

Figure 6 compares the temporal evolutions of rms fluctuations of three velocity components (u_{rms}, v_{rms} and w_{rms}) at $y/M = 0$ and 0.5. Here, the results are also compared among different Fr_M for $Re_M = 10000$. As the turbulence is generated at an early time, the rms velocity fluctuations increase with time. This increase is more rapid at $y/M = 0$ than at $y/M = 0.5$ because the turbulent wake of each plate develops at $y/M = 0$. Then, they begin to decrease as the turbulence decays. At a late time, the rms velocity fluctuations hardly differ at $y/M = 0$ and 0.5 and the flow reaches a statistically homogeneous state. Furthermore, the horizontal velocity fluctuations become isotropic ($u_{rms} \approx v_{rms}$). The time required for stably stratified grid turbulence to be homogeneous and isotropic in the horizontal directions is different depending on Fr_M. This time is about $10t_r$, $20t_r$, $25t_r$ and $10t_r$ for $Fr_M = 0.1$, 0.4, 1 and 6, respectively. For $Fr = 0.1$ and 6, the rms velocity fluctuations monotonically decrease after they reach the peaks. However, u_{rms} and v_{rms} for $Fr_M = 0.4$ and 1 hardly decrease with time for $7 \lesssim t/t_r \lesssim 12$ after the rapid decay from the peak at $t/t_r \approx 4$. This tendency is clearer for $y/M = 0$ in the wakes of vertical plates. Therefore, the slow decay for $7 \lesssim t/t_r \lesssim 12$ might be related to the decay characteristics of the wake.

Figure 7(a) presents u_{rms}/U_0 as a function of time normalized by the buoyancy period N^{-1}. A comparison between figures 6 and 7(a) suggests that the initial growth of rms velocity fluctuations is better characterized by t_r. The time interval corresponding to

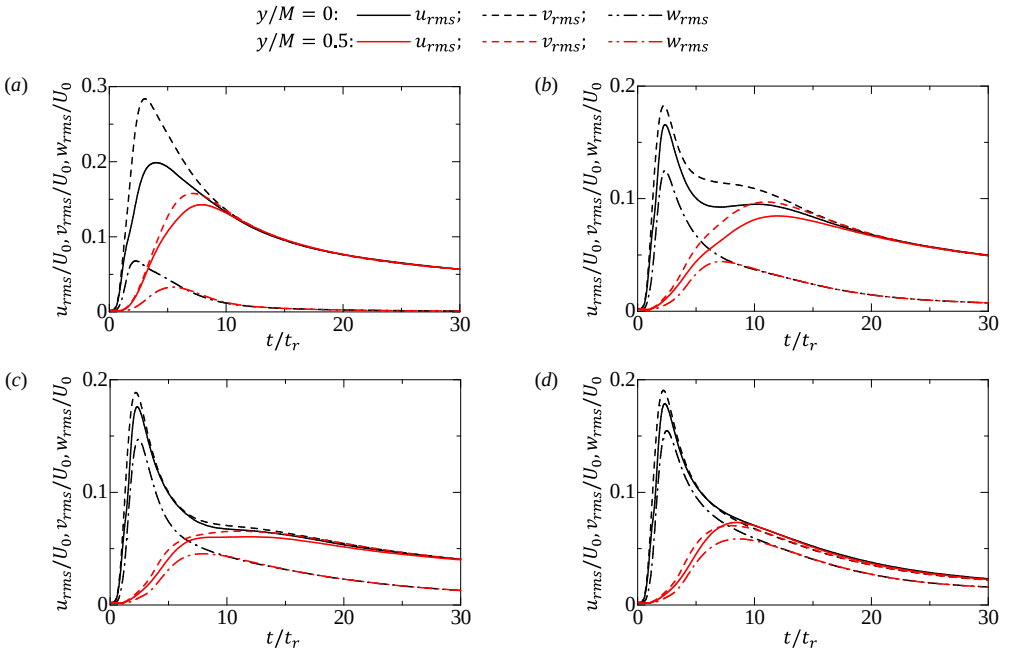

Figure 6: Temporal evolutions of rms velocity fluctuations at $y/M = 0$ and 0.5 in the cases of (a) R10F01, (b) R10F04, (c) R10F1 and (d) R10F6.

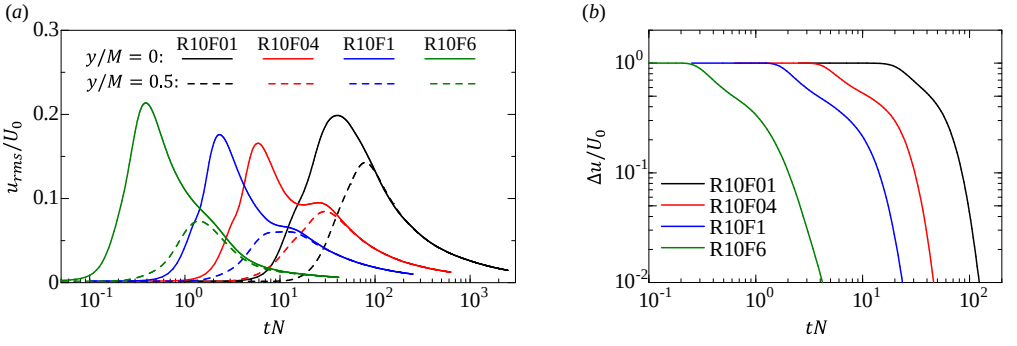

Figure 7: Temporal evolutions of (a) u_{rms}/U_0 at $y/M = 0$ and 0.5 and (b) the mean velocity deficit of the wake, Δu, which are plotted as functions of tN.

the slow decay of u_{rms} is found for $14 \lesssim tN \lesssim 30$ for $Fr = 0.4$ and $7 \lesssim tN \lesssim 20$ for $Fr = 1$. Experiments and numerical simulations of a turbulent wake of a sphere in a stably stratified fluid have reported that the wake development can be divided into three regimes: a three-dimensional regime for $0 \leqslant tN \leqslant 2$; a nonequilibrium (NEQ) regime for $2 \leqslant tN \leqslant 50$; a quasi-two-dimensional regime for $50 \leqslant tN$ (Spedding 1997; Diamessis *et al.* 2011). The decay rates of the mean velocity deficit and rms velocity fluctuations are different among these regimes. Zhou & Diamessis (2019) showed that the decay of the horizontal rms velocity fluctuations becomes slow for $10 \lesssim tN \lesssim 50$, which is within the NEQ regime. In the present DNS, the range of $10 \leqslant tN \leqslant 50$ corresponds to $4 \leqslant t/t_r \leqslant 20$ for $Fr_M = 0.4$ and $10 \leqslant t/t_r \leqslant 50$ for $Fr_M = 1$. The slow decays of u_{rms} and v_{rms} are

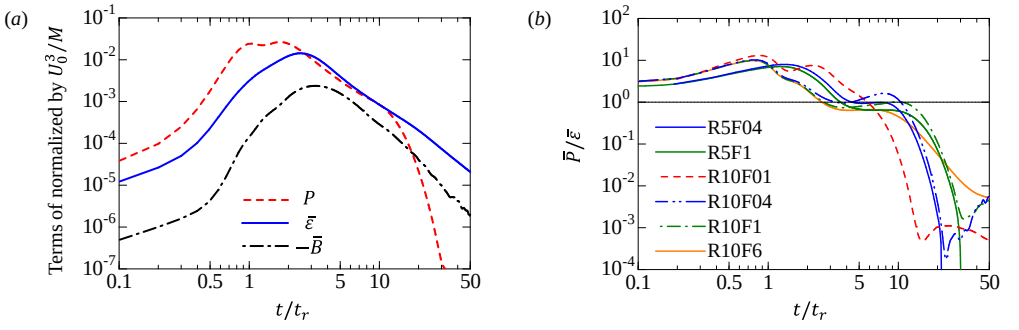

Figure 8: Temporal evolutions of (a) the spatially-averaged budget of turbulent kinetic energy for R10F1 and (b) the ratio between the production and dissipation terms $\overline{P}/\overline{\varepsilon}$.

observed within these intervals. In contrast, the NEQ regime corresponds to $1 \leqslant t/t_r \leqslant 5$ for $Fr_M = 0.1$ and $60 \leqslant t/t_r \leqslant 300$ for $Fr_M = 6$. When the turbulent wake is being generated, u_{rms} at $y = 0$ increases with time. Once the turbulent wake has developed, u_{rms} begins to decay and the interaction of the turbulent wakes generates homogeneous turbulence, where u_{rms} does not depend on y. In figure 7(a), u_{rms} in R10F01 increases with time for the time corresponding to the possible NEQ regime ($10 \lesssim tN \lesssim 50$). Therefore, the NEQ regime is over before the turbulent wake has developed. On the other hand, u_{rms} in R10F6 hardly differs for $y/M = 0$ and 0.5 in the NEQ regime and decreases with time, suggesting that homogeneous turbulence has developed for $Fr_M = 6$ before the wake reaches the NEQ regime. Thus, the slow decay during the NEQ regime of stratified wakes is not observed for $Fr_M = 0.1$ and 6. It should be noted that the discussions are based on the studies on the stratified wake of a sphere, which is different from the wake of a vertical plate considered in this study. The slow decay in the NEQ regime is only one of the possible explanations for the behaviour u_{rms} and v_{rms}.

The wake development of each plate can also be evaluated with the mean velocity deficit Δu, which is defined as the difference in $\langle u \rangle$ between $y/M = 0$ and 1. Figure 7(b) shows Δu as a function of tN. In a freely developing wake of an object, such as a sphere and a cylinder, Δu becomes small with time although Δu does not reach zero. The wakes are generated by many plates in the case of grid turbulence. Therefore, Δu in grid turbulence rapidly decreases to zero with time. In a stably stratified wake of a sphere, the decay of Δu becomes slower once the flow enters the NEQ regime (Spedding 1997). The decay of Δu for R10F04 and R10F1 becomes slightly slower at $tN \approx 10$ and 5, respectively, than at an earlier time. However, the change of the decay rate is less clear than that reported for stably stratified wakes. This might be partially due to the interaction with adjacent wakes, which results in $\Delta u \to 0$ while Δu in a conventional wake is greater than 0 even at a late time.

The budget of the turbulent kinetic energy $k_T(y,t) = (\langle u'^2 \rangle + \langle v'^2 \rangle + \langle w'^2 \rangle)/2$ is examined with the transport equation of k_T. Once the grid turbulence has developed, the production rate of k_T becomes much smaller than the dissipation rate. Here, an average in the y direction is defined for a statistical quantity $F(y,t)$ as $\overline{F}(t) = (1/L_y) \int F(y,t) dy$. The spatially-averaged turbulent kinetic energy $\overline{k_T}$ evolves following the equation given by

$$\frac{d\overline{k_T}}{dt} = \overline{P} - \overline{\varepsilon} + \overline{B}, \tag{4.1}$$

where P, ε and B are the production, dissipation and buoyancy flux in the transport

equation of $k_T(y,t)$:

$$P = -\langle u_i' u_j' \rangle \frac{\partial \langle u_i \rangle}{\partial x_j}, \quad \varepsilon = \nu \left\langle \frac{\partial u_i'}{\partial x_j} \frac{\partial u_i'}{\partial x_j} \right\rangle, \quad B = -\frac{g}{\rho_0} \langle w' \rho' \rangle. \tag{4.2}$$

Here, ε and B are identical to the first and second terms of (2.6), respectively, when the flow is statistically homogeneous. Figure 8(a) shows the temporal evolutions of $\overline{P}$, $\overline{\varepsilon}$ and $\overline{B}$ for R10F1. Initially, $\overline{P}$ is larger than $\overline{\varepsilon}$ until $t/t_r \approx 3$ because the turbulent kinetic energy is initially small and increases due to the production term. Until grid turbulence has developed by the wake interaction, $\overline{P}$ and $\overline{\varepsilon}$ are comparable for $3 \lesssim t/t_r \lesssim 10$. This relationship of $\overline{P} \sim \overline{\varepsilon}$ is widely observed in turbulent free shear flows, where the ratio between the production and dissipation terms of turbulent kinetic energy is close to 1 (Panchapakesan 1993; Taveira & da Silva 2013; Watanabe *et al.* 2016). Then, $\overline{P}$ rapidly decreases because the mean velocity gradient $\partial\langle u \rangle/\partial y$ and the Reynolds stress $\langle u'v' \rangle$ become small as grid turbulence develops into a statistically homogeneous state. Because the buoyancy flux $\overline{B}$ is always negative, $-\overline{B}$ is shown in the figure. Positive values of $-\overline{B}$ suggest that the turbulent kinetic energy is converted to the potential energy. However, $-\overline{B}$ is smaller than $\overline{\varepsilon}$ and the decay of the turbulent kinetic energy is dominated by $\overline{\varepsilon}$. In all DNS, $\overline{\varepsilon}$ is at least 10 times larger than $-\overline{B}$ in the decay period of grid turbulence. Figure 8(b) shows the temporal evolutions of $\overline{P}/\overline{\varepsilon}$. The ratio with $\overline{P}/\overline{\varepsilon} \approx 10^0$ is observed for $3 \lesssim t/t_r \lesssim 10$ except for R10F01, for which $\overline{P}/\overline{\varepsilon}$ begins to decay at an earlier time than for other cases. In all DNS, $\overline{P}/\overline{\varepsilon}$ rapidly decreases because of the development of grid turbulence. However, a comparison between different Fr_M suggests that the rapid decrease of $\overline{P}/\overline{\varepsilon}$ occurs at an earlier time for lower Fr_M. Table 1 includes time t_H at which $\overline{P}/\overline{\varepsilon}$ becomes smaller than 0.01. Beyond this time, turbulence is nearly homogeneous and the production of turbulent kinetic energy is almost negligible. The Reynolds number hardly affects t_H, which increases with Fr_M. Therefore, the grid turbulence reaches a homogeneous state faster under stronger stable stratification.

Figures 9(a,b) present the temporal evolutions of $Fr_H = u_{rms}/L_u N$ and $Re_H = u_{rms} L_u/\nu$ at $y/M = 0$, where L_u is the longitudinal integral scale defined with u. After Fr_H increases by the development of grid turbulence, it monotonically decays. Comparison among all DNS cases suggests that Fr_H depends on Fr_M and does not exhibit a strong dependence on Re_M. Similarly, Re_H reaches a peak when turbulence is generated. However, the decay of Re_H is much slower than that of Fr_H because L_u increases with time. Figure 9(c) shows the buoyancy Reynolds number Re_b at $y/M = 0$. Except for $Fr_M = 0.1$, Re_b exceeds 10 during the turbulence-production phase. Then, Re_b rapidly decreases to $Re_b < 10^0$ for $Fr_M = 0.4$ and 1. However, the grid turbulence with $Fr_M = 6$ has $Re_b > 10^0$ until $t/t_r \approx 70$, and small-scale turbulent motions are active in the early decay period. For $Fr_M = 0.1$, Re_b does not exceed 10^0 even at an early time, and three-dimensional small-scale turbulence is inhibited even when the turbulence is generated.

It is useful to diagnose stably stratified turbulence in the parameter space of (Re_H, Fr_H^{-1}) (Brethouwer *et al.* 2007). Figure 9(d) shows the trajectory of (Re_H, Fr_H^{-1}) during the decay at $y/M = 0$ after the peak of Re_b. The broken lines distinguish four regimes of stratified turbulence proposed in Brethouwer *et al.* (2007): viscosity-affected stratified flow; strongly stratified turbulence; weakly stratified turbulence; classical Kolmogorov turbulence. The two horizontal broken lines represent $Fr_H = 1$ and 0.02 while the diagonal broken line is $Re_H Fr_H^2 = 1$. As discussed above, $Re_H Fr_H^2$ is close to Re_b when $\alpha = \varepsilon/(U_H^3/L_H) \sim 10^0$, and the plots of (Re_H, Fr_H^{-1}) complement the temporal evolution of Re_b. For $(Re_M, Fr_M) = (10000, 6)$, the decay of turbulence begins in the classical Kolmogorov turbulence regime, enters the weakly-stratified turbulence

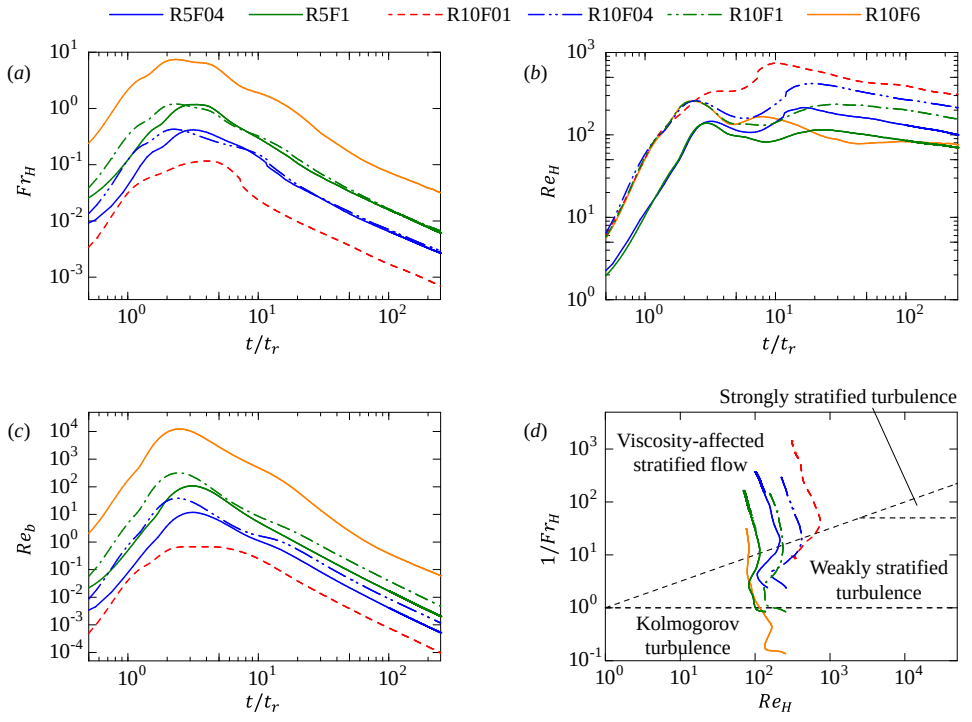

Figure 9: Temporal evolutions of (a) horizontal Froude number Fr_H, (b) Reynolds number based on the horizontal integral scale Re_H and (c) buoyancy Reynolds number Re_b at $y/M = 0$. (d) The relation between Re_H and $1/Fr_H$ during the decay of grid turbulence at $y/M = 0$.

regime and then reaches the viscosity-affected stratified flow regime. For the other cases, the turbulence is generated in the weakly-stratified turbulence regime and the decay proceeds in the viscosity-affected stratified flow regime. The decay of turbulence is examined as a function of time in §4.2. The time at which the flow enters the viscosity-affected stratified flow regime (t_V) is given in table 1. Time t_V is normalized by the reference time scale of grid turbulence t_r or the buoyancy period N^{-1}. For $Re_M = 10000$, $t_V N$ is 80 for both $Fr_M = 0.1$ and 0.4. However, t_V is not determined solely by t_r or N^{-1}.

Figure 10 shows the temporal evolutions of the vertical Froude number $Fr_V = U_H/L_V N$. The theories of strongly stratified turbulence with high Re_b assume that the stable stratification is sufficiently strong, and require large Re_H and small Fr_H in addition to $Re_b \sim Re_H Fr_H^2 \gg 1$. The decay laws for high Re_b are obtained with (2.12), which assumes that Fr_V is independent of time. de Bruyn Kops & Riley (2019) has observed that Fr_V hardly varies with time in decaying turbulence with stable stratification at high Re_H and low Fr_H. In figure 10, Fr_V reaches a maximum value at $t/t_r \approx 10^1$ and decays with time. Therefore, constant Fr_V is not observed in the DNS even though Re_b exceeds 10^2 for large Fr_M cases. This is explained by the weak stratification in these cases, and high Re_b is not a sufficient condition to apply the theories of strongly stratified turbulence.

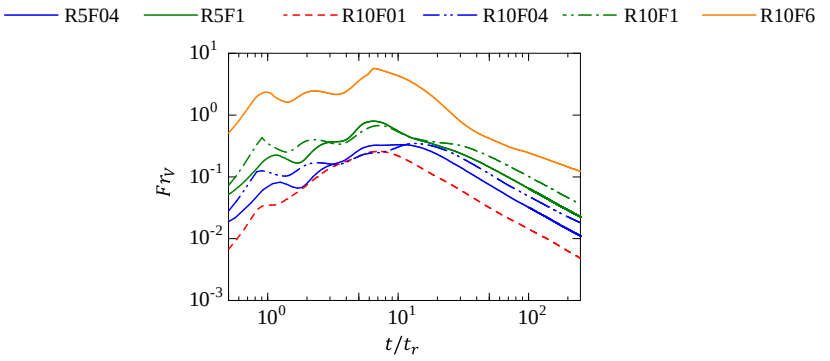

Figure 10: Temporal evolutions of vertical Froude number Fr_V at $y/M = 0$.

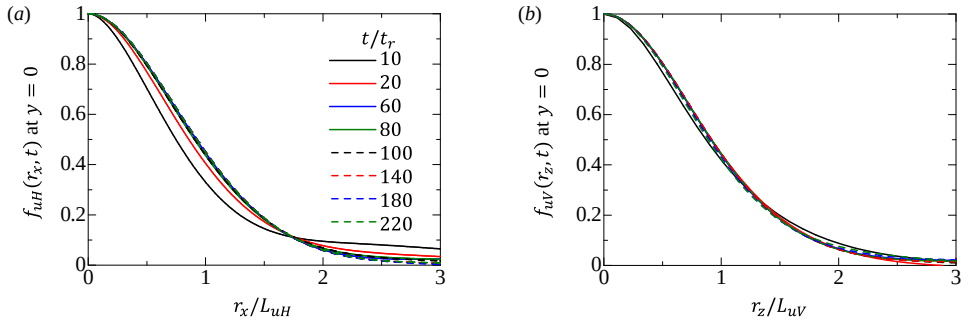

Figure 11: Temporal evolutions of the auto-correlation functions of streamwise velocity defined with separation distances in (a) the streamwise direction, r_x, and (b) the vertical direction, r_z. The results are taken at $y = 0$ for R10F01. The distance is normalized by the integral scale, L_{uH} or L_{uV}.

4.2. *Decay properties of temporally evolving, stably stratified grid turbulence*

The decay of temporally evolving grid turbulence is compared with the theories for Saffman and Batchelor turbulence. The velocity and length scales considered in §2 are defined as follows:

$$U_H = (\langle u'^2 \rangle + \langle v'^2 \rangle)/2,\ L_H = (L_{uH} + L_{vH})/2,\ L_V = (L_{uV} + L_{vV})/2, \tag{4.3}$$

where the horizontal and vertical integral scales of each velocity component are defined as

$$L_{uH} = \int \frac{\langle u'(x,y,z)u'(x+r_x,y,z)\rangle}{\langle u'^2\rangle} dr_x,\ L_{vH} = \int \frac{\langle v'(x,y,z)v'(x,y+r_y,z)\rangle}{\langle v'^2\rangle} dr_y, \tag{4.4}$$

$$L_{uV} = \int \frac{\langle u'(x,y,z)u'(x,y,z+r_z)\rangle}{\langle u'^2\rangle} dr_z,\ L_{vV} = \int \frac{\langle v'(x,y,z)v'(x,y,z+r_z)\rangle}{\langle \langle u'^2\rangle'^2\rangle} dr_z. \tag{4.5}$$

These statistics depend on y and t. Hereafter, the results are presented only for $y/M = 0$ because the statistics are homogeneous during the decay for which the DNS results are compared with the theories.

Time independence of $U_H^2 L_H^4 L_V$ and $U_H^2 L_H^2 L_V$ considered in §2 is derived by

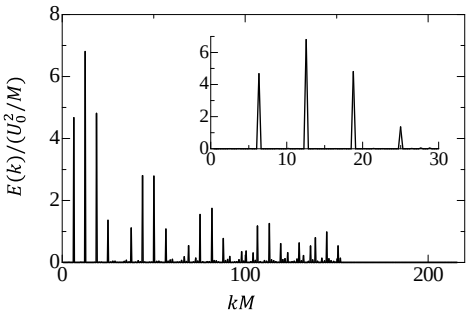

Figure 12: A three-dimensional energy spectrum $E(k)$ at $t = 0$.

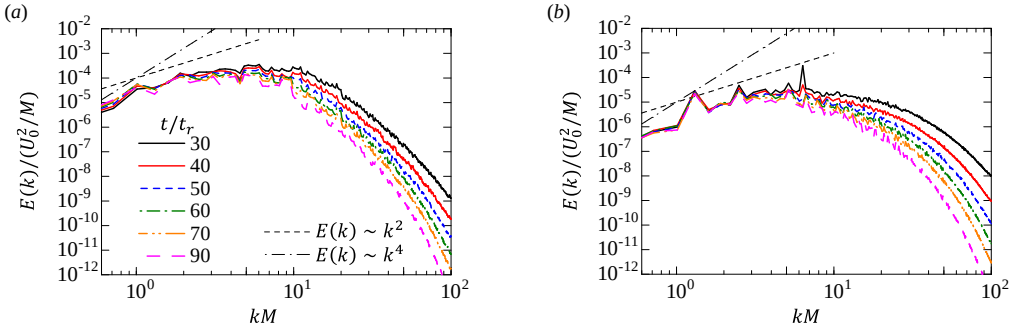

Figure 13: Temporal evolutions of the three-dimensional energy spectrum $E(k)$ for (a) R10F01 and (b) R10F6. The thin black lines represent $E(k) \sim k^2$ and k^4.

the assumption of "partial self-similarity," which means the self-similarity at scales of the order of integral scales (Davidson 2010). If the partial self-similarity is applied, the auto-correlation functions in (4.4) and (4.5) are functions of the separation distance normalized by the integral scale, e.g. r_x/L_{uH}. The assumption of the partial self-similarity is examined with the auto-correlation functions of u, which are denoted by $f_{uH}(r_x, y, t) = \langle u'(x, y, z, t)u'(x + r_x, y, z, t)\rangle/\langle u'^2\rangle$ and $f_{uV}(r_z, y, t) = \langle u'(x, y, z, t)u'(x, y, z+r_z, t)\rangle/\langle u'^2\rangle$. Figure 11 plots f_{uH} and f_{uV} at $y = 0$ as functions of r_x/L_{uH} and r_z/L_{uV}, respectively, in R10F01. For $t/t_r = 10$ and 20, the profiles of f_{uH} vary with time. Similarly, f_{uV} is slightly different between $t/t_r = 10$ and later times. However, the curves collapse well at later times, and f_{uH} and f_{uV} are functions of r_x/L_{uH} and r_z/L_{uV}, respectively, which do not depend on time. The results suggest that the partial self-similarity for large scales is valid except for a very early time.

Saffman turbulence and Batchelor turbulence have a three-dimensional energy spectrum with $E(k) \sim k^2$ and k^4 at large scales, respectively. Axisymmetric turbulence, such as homogeneous turbulence subject to stable stratification or rotation, also has these spectral shapes for Saffman turbulence and Batchelor turbulence. The spectrum in temporally evolving grid turbulence is evaluated with a spherical-shell average following Valente *et al.* (2016). Fourier transform is applied to the instantaneous velocity $u_i(x, y, z, t)$ in the x, y and z directions to obtain the Fourier coefficient $\hat{u}_i(k_x, k_y, k_z, t)$.

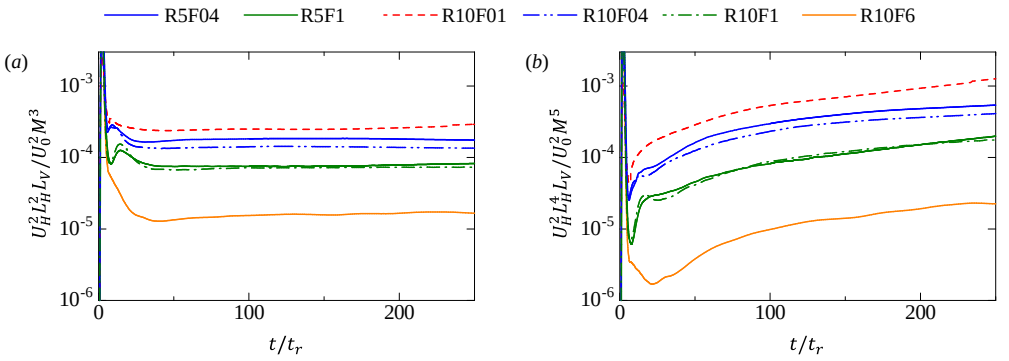

Figure 14: Temporal evolutions of (*a*) $U_H^2 L_H^2 L_V$ and (*b*) $U_H^2 L_H^4 L_V$ at $y/M = 0$.

The energy spectrum is computed as

$$E(k,t) = 4\pi k^2 \left\langle \frac{1}{2} \hat{u}_i \hat{u}_i^* \right\rangle_k , \tag{4.6}$$

where $\hat{u}_i^*$ is the complex conjugate of $\hat{u}_i$, k is the wavenumber, and the spherical-shell average $\langle f \rangle_k$ of $f(k_x, k_y, k_z)$ is defined as

$$\langle f \rangle_k (k) = \frac{1}{N_k} \sum_{|k'-k|<\frac{\Delta k}{2}} f(k_x, k_y, k_z) \quad \text{with} \quad k' = \sqrt{k_x^2 + k_y^2 + k_z^2}. \tag{4.7}$$

Here, the summation is taken for N_k Fourier coefficients whose wavenumber k' satisfies $|k' - k| < \Delta k/2$. The shell thickness is set to be $\Delta k = 0.296 M^{-1}$, which is about 1.4 times larger than the wavenumber of the horizontal domain size $2\pi/L_x = 0.209 M^{-1}$.

Figure 12 shows $E(k)$ of the initial velocity field, where the mean velocity profile is given by (3.5). The wavenumber corresponding to the mesh size M is $k_M = 2\pi/M$. The inset shows $E(k)$ at a low-wavenumber range. Here, $E(k)$ has distinct peaks at wavenumbers related to M, namely $k = k_M$, $2k_M$, $3k_M$ and $4k_M$. The initial velocity field is laminar and does not have the energy spectrum of turbulence, such as $E(k) \sim k^2$ and k^4, which can be formed only after the grid turbulence is generated.

The analysis of the turbulent kinetic energy budget suggests that homogeneous turbulence has developed at $t_H/t_r = 18$–33, as summarized in Table 1. The energy spectrum after $t/t_r = 30$ is examined for the lowest and highest Fr_M cases. Figure 13 shows the temporal evolutions of $E(k)$ for R10F01 and R10F6, which are compared with $E(k) \sim k^2$ and k^4. The oscillation of $E(k)$ is due to statistical convergence because $E(k)$ is evaluated from a single snapshot and small Δk is used to examine $E(k)$ at large scales. For both cases, $E(k)$ for $kM \lesssim 3$ tends to follow $E(k) \sim k^2$ rather than $E(k) \sim k^4$. As turbulence decays with time, $E(k)$ at high wavenumbers becomes small. However, $E(k)$ at low wavenumbers hardly decay with time, suggesting that a coefficient A in $E(k) \approx Ak^2$ is almost independent of time. The time independence of A is related to the linear momentum conservation, which leads to the invariance of Saffman integral (Davidson 2013). Therefore, temporally evolving grid turbulence in a stably stratified fluid evolves following the theory of axisymmetric Saffman turbulence. These results suggest that the mean velocity profile (3.5) results in the formation of Saffman turbulence with $E(k) \sim k^2$ in a stably stratified fluid.

The invariants of Saffman and Batchelor turbulence are examined in figure 14, which presents the temporal evolutions of $U_H^2 L_H^2 L_V$ and $U_H^2 L_H^4 L_V$ at $y/M = 0$. Once the

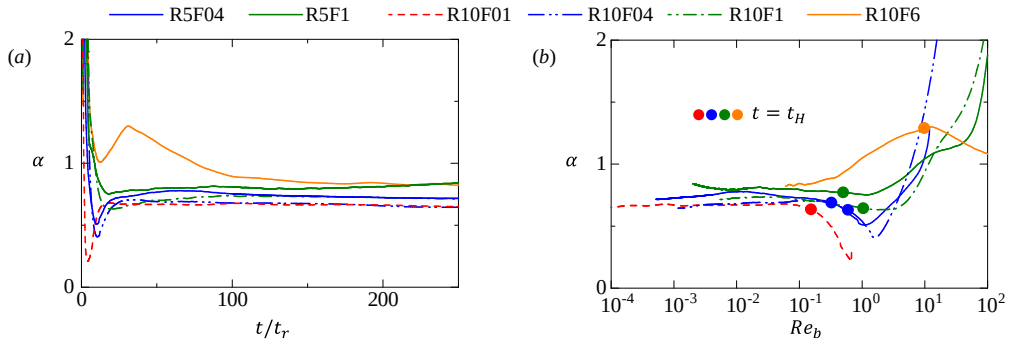

Figure 15: (a) Temporal evolutions of non-dimensional energy dissipation rate $\alpha = \varepsilon/(U_H^3/L_H)$ at $y/M = 0$. (b) α plotted as a function of Re_b at $y/M = 0$. The time after Re_b reaches a peak is plotted in (b).

turbulence is generated, $U_H^2 L_H^2 L_V$ hardly varies while $U_H^2 L_H^4 L_V$ increases with time. Experiments of non-stratified grid turbulence also observed that the invariant of Saffman turbulence, U^2L^3, hardly varies with the distance from the grid while the invariant of the Batchelor turbulence, U^2L^5, monotonically increases as the turbulence decays (Krogstad & Davidson 2010; Kitamura *et al.* 2014). These tendencies agree with the results for $U_H^2 L_H^2 L_V$ and $U_H^2 L_H^4 L_V$ defined for axisymmetric Saffman and Batchelor turbulence. Most wind-tunnel experiments of grid turbulence used conventional square grids, which consist of vertical and horizontal bars while this study considers the rake of vertical plates (Fincham *et al.* 1996; Praud *et al.* 2005). The time independence of $U_H^2 L_H^2 L_V$ indicates that grid turbulence generated by the vertical grid behaves as Saffman turbulence similarly to square-grid turbulence. Comparison of different DNS indicates that $U_H^2 L_H^2 L_V$ becomes independent of time sooner for smaller Fr_M. The turbulent kinetic energy budget in figure 8 also suggests a faster transition to homogeneous turbulence for smaller Fr_M. These results imply that $U_H^2 L_H^2 L_V = $ Const. is achieved after the grid turbulence begins to freely decay without the production of turbulent kinetic energy.

Figure 15(a) presents the temporal variation of the non-dimensional dissipation rate $\alpha = \varepsilon/(U_H^3/L_H)$, which is assumed to be a constant of order 1 in the derivation of the decay laws in §2. After $t/t_r \gtrsim 30$, α hardly varies with time except for R10F6. Although α for R10F6 decreases after it attains the peak, $\alpha \approx 0.85$ tends to be constant for $t/t_r \gtrsim 100$. Although α hardly varies with time in each condition, the values of α depend on Re_M and Fr_M. Therefore, α is not a universal constant in stratified grid turbulence at low Re_b. The values of α for $Fr_M = 0.4$ and 1 slightly depend on Re_M, and α is slightly larger for $Re_M = 5000$. This tendency agrees with DNS of decaying, stably stratified, homogeneous turbulence initialized with a prescribed energy spectrum, where the stationary values of α are larger for lower Reynolds number cases (Maffioli & Davidson 2016). As explained in §2, $\varepsilon = \alpha(U_H^3/L_H)$ for low Re_b is derived with $\varepsilon \sim \nu U_H^2/L_V^2$ and $L_V \sim (\nu L_H/U_H)^{1/2}$. As there are no reasons for prefactors A and B in $\varepsilon = A\nu U_H^2/L_V^2$ and $L_V = B(\nu L_H/U_H)^{1/2}$ to be universal constants which do not depend on flows, $\alpha = A/B^2$ should not be considered as a universal constant. Small temporal variations of α imply that these scalings, $\varepsilon \sim \nu U_H^2/L_V^2$ and $L_V \sim (\nu L_H/U_H)^{1/2}$, are valid during the decay. The decay laws in §2 are derived based on these scalings, which are satisfied by the power laws in (2.19) and (2.20). The results presented below will also show that the temporal evolutions of U_H, L_H, L_V and ε agree with the decay laws of low-Re_b Saffman turbulence except for R10F6, for which α becomes time independent

only at a late time. These results confirm that $\varepsilon \sim \nu U_H^2/L_V^2$ and $L_V \sim (\nu L_H/U_H)^{1/2}$ are satisfied during the decay. Figure 15(b) shows the relationship between α and Re_b. Although Re_b decreases with time, α weakly depends on time. As the flow is not in a strongly stratified turbulence regime, the scaling $\varepsilon \sim U_H^3/L_H$ requires the low-Re_b scaling for L_V and ε. Therefore, α tends to be time-independent only when Re_b is small. However, α in R10F01 varies with time even for $0.1 \lesssim Re_b \lesssim 0.7$. In this range of Re_b, α for other cases varies slowly with Re_b. Filled circles in the figure mark $t = t_H$, before which the flow is statistically inhomogeneous. The time independence of α for R10F01 is achieved only after $t = t_H$. Therefore, $\alpha \approx$ Const. also requires the development of grid turbulence, and $\varepsilon \sim U_H^3/L_H$ seems invalid in the wake of each vertical plate.

The dissipation scaling in non-stratified turbulence can be written as $\varepsilon = C_\varepsilon(U^3/L)$ with the rms velocity fluctuations U and integral length scale L. DNS of statistically steady isotropic turbulence has suggested that $C_\varepsilon = \varepsilon/(U^3/L)$ is a universal constant at a high Reynolds number (Ishihara *et al.* 2009). However, recent studies have confirmed that C_ε differs depending on flows even at high Re (Vassilicos 2015). DNS and experiments suggest that C_ε may vary depending on large-scale flow characteristics, which depend on flows (Mazellier & Vassilicos 2008; Goto & Vassilicos 2016; Takamure *et al.* 2019). Large scales of stratified turbulence should be strongly influenced by the Froude number. For example, pancake-like large-scale vortices are often observed in stratified turbulence (Godoy-Diana *et al.* 2004). The dependence of large scales on Re_M and Fr_M can result in variations of α. Furthermore, wind-tunnel experiments of active-grid turbulence indicate that C_ε are different depending on the grid geometry, the operation mode of the active grid and the Reynolds number although C_ε in each experiment hardly varies with the decay of turbulence (Mora *et al.* 2019; Zheng *et al.* 2021*b*). This behaviour is similar to the evolution of α in figure 15(a) since α in a late time weakly depends on time but differs depending on Re_M and Fr_M. Although the underlying assumption is different for $\varepsilon = C_\varepsilon U^3/L$ in non-stratified turbulence and $\varepsilon = \alpha U_H^3/L_H$ in stratified turbulence, these previous studies of non-stratified turbulence imply that α does not have to be a universal constant.

In all DNS, the flow reaches the viscosity-affected stratified regime during the decay and α hardly varies with time at a late time. Furthermore, $U_H^2 L_H^2 L_V$ also hardly depends on time as suggested from the theory of Saffman turbulence. In the rest of the paper, the decay properties are compared with the theoretical results of low-Re_b Saffman turbulence presented in §2. First, we briefly discuss the decay of main variables and then provide detailed discussions on the decay exponents based on least square estimation.

Figure 16(a) examines the decay of U_H^2, which is compared with the power law $U_H^2 \sim t^{-5/4}$. The slope of U_H^2 is close to the $-5/4$th law except for R10F6. The decay of U_H^2 for R10F6 is slightly slower than $U_H^2 \sim t^{-5/4}$ even for $t/t_r \geqslant 100$, for which the assumptions of constant values of α and $U_H^2 L_H^2 L_V$ are valid. Then, the deviation from $U_H^2 \sim t^{-5/4}$ should be attributed to the validity of (2.18), which may not be valid when Fr_M is not sufficiently low. It is also clear that the decay exponent of R10F6 is not constant for $30 \lesssim t/t_r \lesssim 100$ because α also varies with time although the grid turbulence has fully developed by $t/t_r = 30$. Figure 16(b) shows the variation of the kinetic energy dissipation rate ε. As expected for Saffman turbulence with low Re_b, the present DNS results with $Fr_M \leqslant 1$ follow $\varepsilon \sim t^{-9/4}$ during the decay.

Figures 17(a, b) show the variations of integral scales, L_H and L_V. The Re_M dependence is weak for L_H, which is more dependent on Fr_M. The increase of L_H follows $L_H \sim t^{3/8}$ from $t/t_r \approx 20$ except for R10F6, for which $L_H \sim t^{3/8}$ is valid only after $t/t_r \approx 100$. Although L_V depends on both Re_M and Fr_M at an early time, it hardly depends on Re_M at a late time as the lines for different Fr_M converge to a single line.

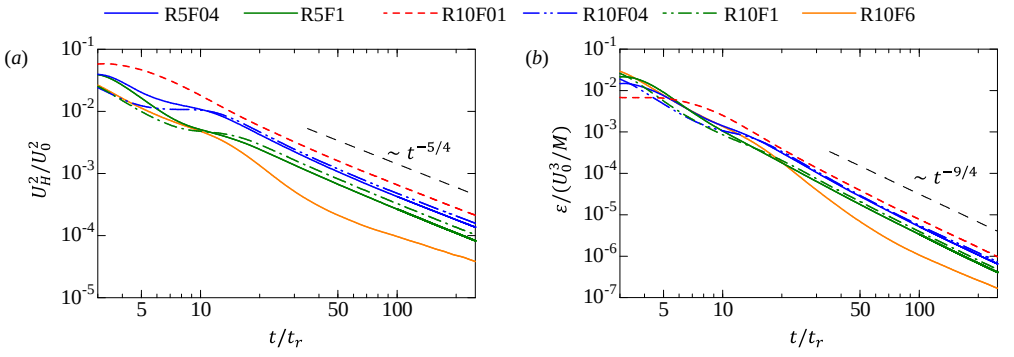

Figure 16: Decay of (a) horizontal velocity fluctuations U_H^2 and (b) turbulent kinetic energy dissipation rate ε at $y/M = 0$.

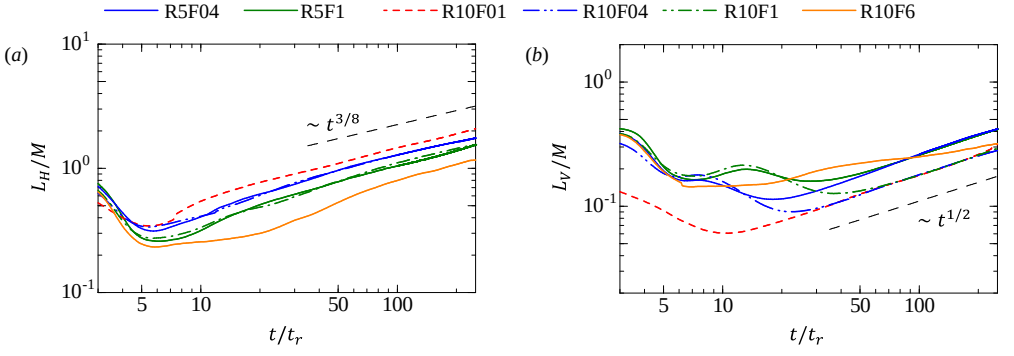

Figure 17: Temporal evolutions of (a) horizontal and (b) vertical integral length scales at $y/M = 0$.

The DNS results with $Fr_M \leqslant 1$ follow $L_V \sim t^{1/2}$. However, $L_V \sim t^{1/2}$ tends to prevail at a later time than $L_H \sim t^{3/8}$ especially for higher Fr_M. For R10F6, the exponent is different from 1/2 even at the end of the simulation.

Turbulence is initially generated as turbulent wakes, whose interaction results in the formation of grid turbulence. Therefore, the flow behaviour at an early time can be related to that of stably stratified turbulent wakes. For an axisymmetric wake generated by a sphere or a disk, the characteristic length of large scales is often defined with the spatial distribution of mean velocity deficit or turbulent kinetic energy (Diamessis *et al.* 2011; Chongsiripinyo & Sarkar 2020). DNS of the stably stratified wake of a disk shows that both horizontal and vertical length scales slightly decrease when the turbulent wake is being generated (Chongsiripinyo & Sarkar 2020). Once the wake becomes turbulent, these length scales increase as the wake evolves. These evolutions of the length scales are similar in figure 17, and the wake length scales defined with mean velocity or turbulent kinetic energy can be related to the integral scales defined with the auto-correlation functions of horizontal velocity.

Figure 18(a) examines the decay of potential energy E_P. The present DNS results exhibit wavelike oscillations of E_P as also found in previous DNS (de Bruyn Kops & Riley 2019). This can be confirmed from the inset of figure 18(a), where E_P between $t/t_r = 105$ and 107 is shown for R10F01 in a linear plot. However, the amplitude of the oscillation is much smaller than the variation of E_P during the decay, for which E_P

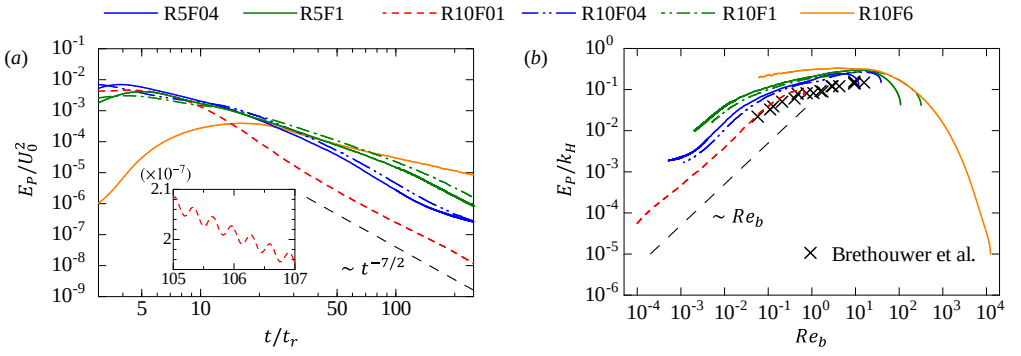

Figure 18: (a) Decay of potential energy E_P at $y/M = 0$. (b) The buoyancy Reynolds number dependence of the ratio between the potential and horizontal kinetic energies E_P/k_H. The trajectory in $(Re_b, E_P/k_H)$ space at $y/M = 0$ is shown after Re_b reaches a peak. DNS results of forced, stably stratified homogeneous turbulence are also shown for comparison (Brethouwer *et al.* 2007).

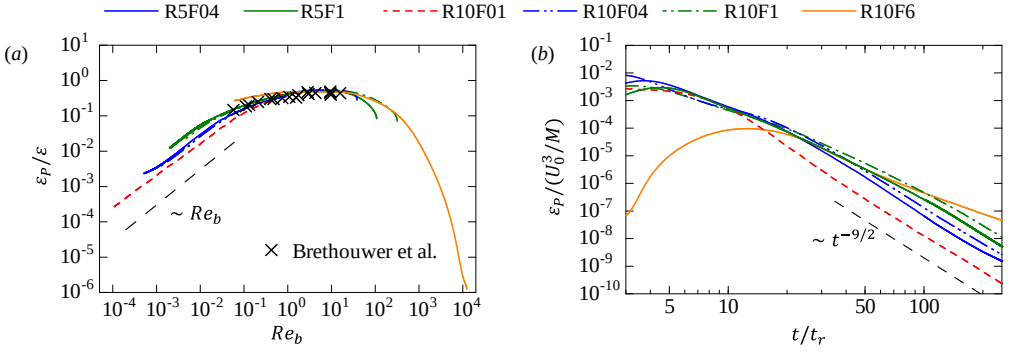

Figure 19: (a) The buoyancy Reynolds number dependence of the ratio between the dissipation rates of potential energy and kinetic energy $\varepsilon_P/\varepsilon$. The results are shown after the peak of Re_b. DNS results of forced, stably stratified homogeneous turbulence are also shown for comparison (Brethouwer *et al.* 2007). (b) Decay of potential energy dissipation rate ε_P. All results are taken at $y/M = 0$.

decreases from $E_P/U_0^2 = \mathcal{O}(10^{-3})$ to $\mathcal{O}(10^{-8})$. Therefore, the wavelike oscillation of E_P is not visible in the logarithmic plot and does not affect the overall decay rate of E_P. The decay for $Fr_M = 0.1$ and 0.4 tends to follow the power law of $E_P \sim t^{-7/2}$. However, a deviation from $E_P \sim t^{-7/2}$ is found for $Fr_M = 0.4$ after $t/t_r \approx 150$. The power law $E_P \sim t^{-7/2}$ assumes (2.15) and (2.18), which can be used to derive $E_P/k_H \sim Re_b$ for the ratio of E_P to the horizontal kinetic energy $k_H = U_H^2$. Figure 18(b) plots the relation between Re_b and E_P/k_H after Re_b reaches a peak. The present DNS results are compared with the DNS of forced, stably stratified homogeneous turbulence in Brethouwer *et al.* (2007). Below $Re_b \approx 10$, E_P/k_H decreases with Re_b being small. The ratio E_P/k_H for $Fr_M = 0.1$ tends to follow $E_P/k_H \sim Re_b$ for $Re_b \lesssim 10^{-1}$. Although this relation is found for $Re_b \approx 10^{-2}$ in the cases of $Fr_M = 0.4$, the DNS data deviate from $E_P/k_H \sim Re_b$ at a lower Re_b. For R10F01, $E_P/k_H \sim Re_b$ is valid for a wide range of Re_b and therefore the decay of E_P approximately follows $E_P \sim t^{-7/2}$.

Although the discussion in §2 does not provide the decay law of the potential energy

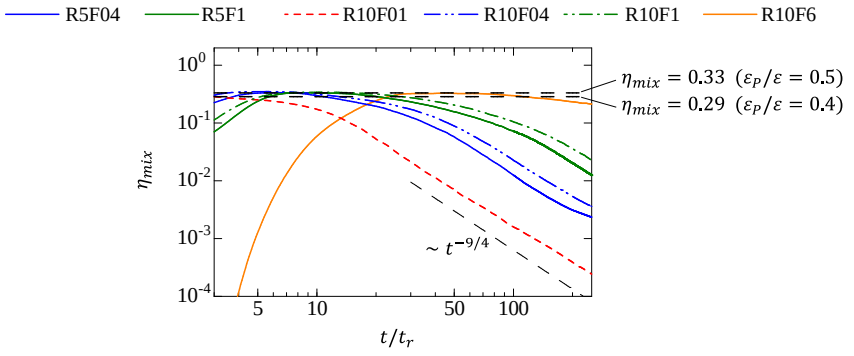

Figure 20: Temporal variation of mixing efficiency $\eta_{mix} = \varepsilon_P/(\varepsilon + \varepsilon_P)$ at $y/M = 0$. Horizontal broken lines represent η_{mix} with $\varepsilon_P/\varepsilon = 0.4$ and 0.5.

dissipation rate ε_P, the decay law in a form of $\varepsilon_P \sim t^n$ may be empirically established because the ratio $\varepsilon_P/\varepsilon$ often depends on Re_b (Brethouwer *et al.* 2007). Figure 19(a) shows the relation between Re_b and $\varepsilon_P/\varepsilon$, which is compared again with DNS by Brethouwer *et al.* (2007). For $Re_b \gtrsim 10^{-1}$, the variation of $\varepsilon_P/\varepsilon$ with Re_b is consistent between decaying grid turbulence and forced homogeneous turbulence. For $Re_b \lesssim 10^{-1}$, $\varepsilon_P/\varepsilon$ decreases as Re_b becomes small. The present data roughly follows $\varepsilon_P/\varepsilon \sim Re_b$ for $Re_b \lesssim 10^{-2}$. This relation $\varepsilon_P \sim \varepsilon Re_b = \varepsilon^2/N^2\nu$ combined with the decay laws of ε in (2.19) and (2.20) yields

$$\varepsilon_P \sim t^{-9/2} \quad \text{for low-}Re_b \text{ Saffman turbulence,} \tag{4.8}$$

$$\varepsilon_P \sim t^{-5} \quad \text{for low-}Re_b \text{ Batchelor turbulence.} \tag{4.9}$$

An alternative way to derive these decay laws is neglecting the buoyancy flux term in (2.7), and $dE_P/dt = -\varepsilon_P$ with (2.21) and (2.22) yields (4.8) and (4.9), respectively. Indeed, the wavelike oscillation of E_P arising from the buoyancy flux was shown to be smaller than the overall decay of E_P in figure 18(a). Figure 19(b) compares the decay of ε_P with $\varepsilon_P \sim t^{-9/2}$. The present DNS data except for R10F6 follows $\varepsilon_P \sim t^{-9/2}$ derived based on the empirical relation $\varepsilon_P \sim \varepsilon Re_b$ combined with the decay law of Saffman turbulence.

It should be noted that $\varepsilon_P \sim \varepsilon Re_b$ is valid only when Re_b is sufficiently small. Figure 19(a) suggest that $\varepsilon_P/\varepsilon$ weakly depends on Re_b for $1 \lesssim Re_b \lesssim 10$. Strong Re_b-dependence of $\varepsilon_P/\varepsilon$ is observed for $Re_b \gtrsim 10^1$. This range of Re_b is in the production phase of grid turbulence and the grid turbulence has not fully developed yet. Brethouwer *et al.* (2007) also observed that $\varepsilon_P/\varepsilon = 0.4$-$0.5$ hardly depends on Re_b when $Re_b \sim Re_H Fr_H^2 > 1$. Similar values of $\varepsilon_P/\varepsilon$ were also reported by Riley & de Bruyn Kops (2003), Lindborg (2006) and Maffioli & Davidson (2016). If $\varepsilon_P/\varepsilon$ is constant during the decay, the decay exponent of ε_P is the same as that of ε. The relation $\varepsilon_P \sim \varepsilon$ might be useful at a high-Re_b regime, for which one can derive the following decay laws of ε_P

$$\varepsilon_P \sim t^{-9/5} \quad \text{for high-}Re_b \text{ Saffman turbulence,} \tag{4.10}$$

$$\varepsilon_P \sim t^{-15/7} \quad \text{for high-}Re_b \text{ Batchelor turbulence,} \tag{4.11}$$

from (2.13) and (2.14). However, the Reynolds number is not large enough in the present DNS to verify these decay laws.

One of the important parameters in oceanography is mixing efficiency that is often defined as $\eta_{mix} = \varepsilon_P/(\varepsilon + \varepsilon_P) = (1 + \varepsilon/\varepsilon_P)^{-1}$ (Smyth *et al.* 2001; Gregg *et al.* 2018).

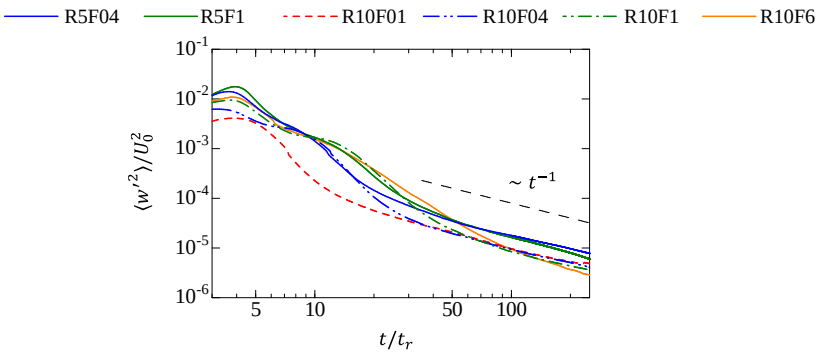

Figure 21: Decay of vertical velocity variance $\langle w'^2\rangle$ at $y/M = 0$.

DNS of stably stratified turbulence has been utilized to parametrize η_{mix} (Salehipour *et al.* 2015; Maffioli *et al.* 2016; de Bruyn Kops & Riley 2019; VanDine *et al.* 2021). If $\varepsilon_P/\varepsilon$ is constant during the decay, η_{mix} does not vary with time. However, the decay laws derived for low-Re_b Saffman and Bachelor turbulence suggest that η_{mix} decays with time as $\eta_{mix} \sim (1+t^{9/4})^{-1}$ for Saffman turbulence and $\eta_{mix} \sim (1+t^{5/2})^{-1}$ for Batchelor turbulence. As long as the late time behaviour of grid turbulence is concerned, we may approximate these decay laws as

$$\eta_{mix} \sim t^{-9/4} \quad \text{for low-}Re_b\text{ Saffman turbulence,} \tag{4.12}$$

$$\eta_{mix} \sim t^{-5/2} \quad \text{for low-}Re_b\text{ Batchelor turbulence.} \tag{4.13}$$

Figure 20 shows the temporal variation of η_{mix} compared with (4.12). As expected, η_{mix} decreases as turbulence decays. Before the decay of η_{mix} begins, η_{mix} is about 0.33, which is close the values corresponding to $\varepsilon_P/\varepsilon = 0.4$-$0.5$ and is consistent with other DNS studies of stratified homogeneous turbulence (de Bruyn Kops & Riley 2019). The decay of η_{mix} tends to follow (4.12) although $\eta_{mix} \sim t^{-9/4}$ is observed at a later time for higher Fr_M. de Bruyn Kops & Riley (2019) also found in DNS of decaying, stably stratified homogeneous turbulence that η_{mix} stays at an almost constant value at an early time of the decay with high Re_b and then decreases with time once Re_b becomes small although this decay was not emphasized in their paper.

Figure 21 shows the decay of vertical velocity variance $\langle w'^2\rangle$. The theories for stably stratified turbulence in §2 concerns large-scale characteristics of the flow and do not provide the decay law of $\langle w'^2\rangle$, which is dominated by small-scale fluctuations in stratified turbulence. However, $\langle w'^2\rangle$ tends to follow $\langle w'^2\rangle \sim t^{-1}$ except for R10F6. Towed-grid experiments by Praud *et al.* (2005) also observed $\langle w'^2\rangle \sim t^{-1}$ at low Fr_M.

These results suggest that temporally evolving grid turbulence in a stratified fluid behaves similarly to Saffman turbulence. Previous numerical studies of Saffman turbulence and Batchelor turbulence consider decaying turbulence initialized with a velocity field that satisfies $E(k) \sim k^2$ or k^4 at large scales (Ishida *et al.* 2006; Teitelbaum & Mininni 2012; Yoshimatsu & Kaneda 2018; de Bruyn Kops & Riley 2019; Anas *et al.* 2020). It has been shown that the decay of turbulence with the k^2 and k^4 spectra is consistent with the theories of Saffman and Batchelor turbulence, respectively. However, these studies do not reveal how turbulence with $E(k) \sim k^2$ or k^4 is generated because the energy spectrum is imposed as the initial condition. The temporally evolving grid turbulence is initialized with a laminar flow that approximates the mean velocity deficit of the wakes. Therefore, the production of turbulence occurs simply due to the mean velocity gradient imposed

as the initial condition. The results presented above imply that the mean velocity deficit caused by the grid is essential for grid turbulence to behave like Saffman turbulence.

4.3. *Estimation of decay exponents*

The results shown above indicate that most quantities vary with time in accord with a power law of t. From experiments and numerical simulations of grid turbulence with and without stable stratification, it is widely accepted that the decay of horizontal velocity fluctuations follows

$$\frac{U_H^2}{U_0^2} = A\left(\frac{t}{t_r} - \frac{t_0}{t_r}\right)^n, \tag{4.14}$$

where t_0 is the virtual origin. Various methods have been proposed to determine the unknown parameters A, t_0 and n from data taken in laboratory experiments of non-stratified grid turbulence (Lavoie *et al.* 2007; Krogstad & Davidson 2010; Valente & Vassilicos 2011). Most methods provide a similar decay exponent n although small variations may exist because the virtual origin is determined in a different manner. These methods are based on linear or nonlinear least square estimation applied to a certain range of decay. It is known that the fitting range $t_s \leqslant t \leqslant t_e$ may significantly affect n in non-stratified grid turbulence, where t_s and t_e are the start and end points (time) of the fitting range. As discussed in the introduction, a near-grid region has a faster decay rate than a fully-developed turbulence region (Komori *et al.* 1993; Krogstad & Davidson 2012). Furthermore, n also increases as turbulence decays to a low Reynolds number regime. Here, the variation of n is often explained by that of C_ε. Except for R10Fr6 the temporal variation of $\alpha = \varepsilon/(U_H^3/L_H)$ in figure 15 is large for $t/t_r \lesssim 20$, which may correspond to the non-equilibrium decay region in the case of non-stratified grid turbulence generated by a square grid (Isaza *et al.* 2014; Nagata *et al.* 2017). Therefore $t/t_r \lesssim 20$ should be eliminated from the data used to estimate n. Furthermore, the power law of L_V predicted for low Re_b seems valid for $t/t_r \gtrsim 20$ for $Fr = 0.1$, $t/t_r \gtrsim 30$ for $Fr = 0.4$ and $t/t_r \gtrsim 60$ for $Fr = 1$ in figure 17(b). By taking these points into consideration, $t_s/t_r = 70$ is adapted except for R10F6. We have also confirmed that the decay exponents obtained with larger t_s hardly differ from those with $t_s/t_r = 70$. The assumption of constant α becomes valid only after $t \approx 100$ for R10F6, and n is estimated with $t_s/t_r = 120$. In all cases, the fitting range is within the viscosity-affected stratified flow regime. Experiments at very large t/t_r (x/M) often have a difficulty in dealing with background velocity fluctuations that can be comparable to turbulent fluctuations and with measurement errors arising from, for example, electronic noise of hot-wire anemometry. Therefore, the end point of the fitting range has to be carefully determined in experiments. However, these issues do not affect the estimation of n in numerical simulations. Furthermore, the decay of turbulence in a stably stratified fluid does not result in the increase of α, which is almost constant even in a late time. The estimation of n in stratified grid turbulence is not as sensitive to t_e as in experiments of non-stratified grid turbulence. Therefore, t_e is set as the end of the computations, i.e. $t_e/t_r = 250$.

This study compares n obtained by three methods explained here. Method 1 predetermines t_0/t_r and applies a linear least square method to the DNS data of $(U_H^2/U_0^2, t/t_r - t_0/t_r)$ in a form of $\ln(U_H^2/U_0^2) = \ln A + n\ln(t/t_r - t_0/t_r)$, for which $\ln A$ and n are analytically determined. The fitting is repeatedly applied by changing t_0/t_r from -100 to 100 with an increment of 0.1. The virtual origin t_0/t_r is determined such that the standard deviation of the DNS data from the fitting function is the smallest for all tested virtual origins. This virtual origin is used to determine $\ln A$ and n with the linear least square method. The condition of the minimum standard deviation is often used to determine

Table 2: Decay exponents and virtual origins estimated by three different methods.

Run	Method 1		Method 2		Method 3	
	n	t_0/t_r	n	t_0/t_r	n	t_0/t_r
R5F04	−1.21	3.8	−1.24	0	−1.27	−0.70
R5F1	−1.23	6.2	−1.29	0	−1.22	4.16
R10F01	−1.19	5.0	−1.24	0	−1.31	−6.06
R10F04	−1.17	5.5	−1.22	0	−1.16	5.34
R10F1	−1.20	7.4	−1.27	0	−1.22	6.16
R10F6	−0.90	17.7	−1.00	0	−0.93	11.4

one of the fitting parameters, e.g. a range of t (or x in wind-tunnel experiments) where the least square method is applied to calculate n (Krogstad & Davidson 2010; Kitamura *et al.* 2014). Method 2 assumes that the virtual origin is equal to zero and the linear least square method is applied for $\ln(U_H^2/U_0^2) = \ln A + n\ln(t/t_r)$ to determine $\ln A$ and n. This method yields the decay exponent equivalent to those considered in some previous studies on stably stratified grid turbulence, where the decay exponent was obtained for $(U_H^2/U_0^2) = A(t/t_r)^n$ with the assumption of $t_0 = 0$ (Liu 1995; Praud *et al.* 2005; Espa *et al.* 2018). Method 3 directly applies a nonlinear least square method (Levenberg-Marquardt method) to simultaneously determine A, t_0/t_r and n of (4.14). The nonlinear least square method has been widely used for experimental data of grid turbulence and was shown to provide n consistent with other methods (Valente & Vassilicos 2011; Isaza *et al.* 2014; Kitamura *et al.* 2014; Zheng *et al.* 2021*a*).

Table 2 summarizes the decay exponent and virtual origin obtained by the three methods. Exponent n for R10F6 is smaller than for the other cases as also expected from the slower decay of R10F6 in figure16(*a*). However, n for $Fr = 0.1$, 0.4 and 1 is close to $n = -1.25$ derived for low-Re_b Saffman turbulence. Although each method yields different virtual origins, the estimated values of n differ only slightly. This weak sensitivity of n to the choice of t_0 is related to the fitting range that includes large t/t_r up to 250 because the decay exponent estimated from data at large t/t_r is known to be insensitive to small variations of the virtual origin (Zheng *et al.* 2021*a*). The variations of n found among the three methods are at a similar level to experimental results of non-stratified grid turbulence (Valente & Vassilicos 2011). Averages of n taken except for R10F6 are −1.20, −1.25 and −1.23 for methods 1, 2 and 3 respectively. These values are fairly close to the prediction $n = -1.25$ for low-Re_b Saffman turbulence.

The DNS results suggest that a power law $f = A(t - t_0)^n$ is also valid for various quantities shown in figures 16-19. Exponent n is estimated by applying the linear least square method to $\ln f = \ln A + n\ln(t - t_0)$ with the virtual origin estimated from U_H^2 by method 1. Table 3 summarizes the estimated values of n for the integral scales, potential energy and dissipation rates of kinetic and potential energies. The exponents for L_H, L_V and ε are close to the values for low-Re_b Saffman turbulence except for R10F6. The faster growth of L_V than L_H is also found for DNS data as predicted for low-Re_b Saffman turbulence. The decay of E_P and ε_P of the DNS data tends to be slower than low-Re_b Saffman turbulence although the difference from the theory is not large for some cases, e.g. R10F04 and R10F01. This is because the exponents of $E_P/k_H \sim Re_b^p$ and

Table 3: Power-law exponents of integral scales, potential energy and dissipation rates of kinetic and potential energies.

Run	t_0/t_r	Power-law exponent n				
		L_H	L_V	ε	E_P	ε_P
R5F04	3.8	0.34	0.51	−2.21	−2.56	−4.06
R5F1	6.2	0.40	0.50	−2.22	−3.00	−4.09
R10F01	5.0	0.37	0.54	−2.17	−3.12	−4.16
R10F04	5.5	0.33	0.48	−2.13	−3.15	−4.15
R10F1	7.4	0.37	0.50	−2.18	−2.59	−3.71
R10F6	17.7	0.38	0.26	−1.78	−1.26	−2.23
Saffman turbulence with low Re_b		0.375	0.5	−2.25	−3.5	−4.5

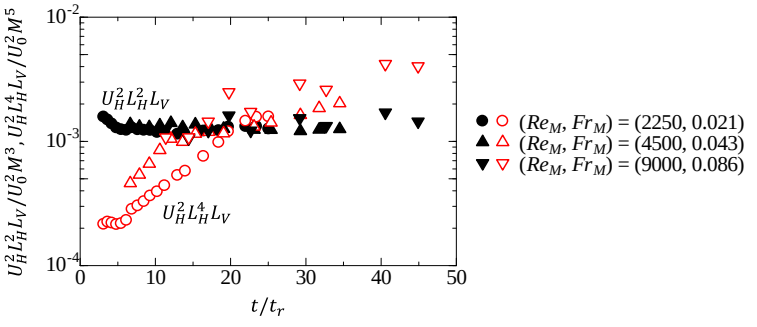

Figure 22: Temporal evolutions of $U_H^2 L_H^2 L_V$ and $U_H^2 L_H^4 L_V$ in experiments of towed-grid turbulence in Praud *et al.* (2005).

$\varepsilon_P/\varepsilon \sim Re_b^p$ deviate from $p = 1$ especially for large Re_b while $n = -3.5$ for E_P and -4.5 for ε_P require $p = 1$.

5. Decay properties of stably stratified grid turbulence: a review of experimental data

The present DNS results have confirmed that the decay of temporally evolving, stably stratified grid turbulence is consistent with the theory for low-Re_b Saffman turbulence. It is natural to consider that whether decaying homogeneous turbulence obeys the decay laws of Saffman turbulence or Batchelor turbulence depends on the generation process of turbulence (Davidson 2004). Therefore, it is also important to compare the present findings with experimental data because the temporal grid turbulence is only an approximation of actual grid turbulence studied in laboratories.

Praud *et al.* (2005) presented the measurement results of horizontal kinetic energy and horizontal and vertical integral scales for turbulence generated by a towed rake of vertical plates for $1125 \leqslant Re_M \leqslant 36000$ and $0.021 \leqslant Fr_M \leqslant 0.36$. The parameter ranges

of (Re_M, Fr_M) are similar to the present DNS although their Schmidt number is larger than 1 because the experiments were conducted with saltwater. The decay laws of low-Re_b Saffman turbulence are expected for their experiments. Although other experimental studies also investigated stratified grid turbulence for similar values of (Re_M, Fr_M), the number of data points in the plot of U_H^2 is not enough to assess the decay rate or the horizontal and vertical integral scales are not available (Itsweire *et al.* 1986; Fincham *et al.* 1996; Yap & Van Atta 1993). Therefore, we present comparisons with low-Re_b Saffman turbulence only for Praud *et al.* (2005). Figure 22 shows temporal variations of $U_H^2 L_H^2 L_V$ and $U_H^2 L_H^4 L_V$ in their experiments, which are constant for Saffman turbulence and Batchelor turbulence, respectively. As also observed in the present DNS, $U_H^2 L_H^2 L_V$ hardly varies with time while $U_H^2 L_H^4 L_V$ increases. Thus, the grid turbulence investigated in their facility also behaves as axisymmetric Saffman turbulence. They also observed that the decay of U_H^2 measured under various conditions follows $U_H^2 \sim t^{-1.3}$, which is close to $t^{-1.25}$ of low-Re_b Saffman turbulence. We estimate the decay exponent of horizontal kinetic energy U_H^2 from one of their experiments with $(Re_M, Fr_M) = (9000, 0.086)$, for which U_H^2 was measured for $30 \lesssim t/t_r \lesssim 150$. We have obtained $n = -1.31$ and $t_0/t_r = 8$ for $U_H^2/U_0^2 = A(t/t_r - t_0/t_r)^n$ by applying the maximum decay range method (Lavoie *et al.* 2007). For the same experiment with $(Re_M, Fr_M) = (9000, 0.086)$, we have obtained $L_H \sim (t/t_r - 8)^{0.30}$ and $L_V \sim (t/t_r - 8)^{0.48}$ with the least square method. Furthermore, they also estimated the kinetic energy dissipation rate ε based on the gradients of horizontal velocity and found that ε decays as $\varepsilon \sim t^{-2.3}$. These power-law exponents in their experiments are close to the values of low-Re_b Saffman turbulence. The slower growth of L_H than L_V is also consistent with the theoretical prediction. Thus, their experimental results are explained well by the decay laws derived for low-Re_b Saffman turbulence.

Experiments of stably stratified grid turbulence have also been conducted for higher Fr_M than Praud *et al.* (2005). Itsweire *et al.* (1986) presented the measurement results of U_H^2 in grid turbulence with $Fr_M \approx$ 7-15 in a ten-layer, salt-stratified water channel. They found that the decay of U_H^2 in stratified grid turbulence is faster than in non-stratified cases. Similarly, Liu (1995) also reported that the decay becomes faster by the stable stratification in experiments of towed-grid turbulence in a linearly stratified fluid for $Fr_M = 40$ and 80. On the other hand, water-channel experiments of grid turbulence with a stable linear density gradient by Stillinger *et al.* (1983) observed the opposite effect on U_H^2 for $Fr_M \approx$ 14-29: the decay becomes slow by the influence of stable stratification. Lienhard & van Atta (1990) conducted wind-tunnel experiments of thermally stratified grid turbulence with a linear density profile for $Fr_M \approx$ 17-42. However, they did not find significant influences of stable stratification on the decay of U_H^2. Similarly, for grid turbulence in a two-layer, density stratified water, Huq & Britter (1995) and Komori & Nagata (1996) reported that the decay rate of U_H^2 was hardly influenced by the stable stratification for $Fr_M \approx 3$. These studies observed different influences of stable stratification on the decay of horizontal velocity fluctuations for $Fr_M = \mathcal{O}(10^0\text{-}10^1)$. The present DNS of R10F6 suggests that the decay rate of U_H^2 varies with time in figure 16(a), where the least square method yields $U_H^2/U_0^2 \sim (t/t_r)^{-2.3}$ for $15 \leqslant t/t_r \leqslant 40$ and $U_H^2/U_0^2 \sim (t/t_r)^{-1}$ at a later time. The Saffman turbulence without density stratification decays as $U_H^2/U_0^2 \sim (t/t_r)^{-1.2}$. Thus, the decay rate for $Fr_M = 6$ is faster in the early time than for the non-stratified case and slower in the late time, and the decay exponent is not constant during the decay. Furthermore, R10F6 also suggests that the non-dimensional dissipation rate α is not constant in the early time of decay until $t/t_r \approx 100$. The time independence of α is the basis of the power law of U_H^2 with a constant exponent n. This is possibly related varieties of the stratification influences on the decay reported in

previous experiments with $Fr_M = \mathcal{O}(10^0\text{-}10^1)$ because most experiments were conducted for $t/t_r \leqslant 100$ ($x/M \leqslant 100$).

6. Conclusion

The decay of stably stratified grid turbulence generated by a rake of vertical plates was investigated by DNS of temporally evolving grid turbulence in a linearly stratified fluid. DNS was performed for $Re_M = 5000$ and 10000 and $Fr_M = 0.1\text{-}6$. The theories for decaying, stably stratified homogeneous turbulence based on axisymmetric Saffman and Batchelor turbulence by Davidson (2009, 2010) were extended to a viscosity-affected stratified flow regime characterized by low Re_b. The extended theories predicted the power-law behaviours of the horizontal velocity scale of large-scale motions U_H and the horizontal and vertical integral scales, L_H and L_V. Here, the derivations were based on the invariant properties of axisymmetric Saffman and Batchelor turbulence, which are written as $U_H^2 L_H^2 L_V = \text{Const.}$ and $U_H^2 L_H^4 L_V = \text{Const.}$, respectively. The power laws of U_H, L_H and L_V were obtained by combining these constraints during the decay with the scaling of the kinetic dissipation rate $\varepsilon = \alpha(U_H^3/L_H)$ with a constant α and the low-Re_b scaling of the vertical scale, $L_V \sim L_H Re_H^{-1/2}$. In addition, the decay laws of potential energy were derived with the scaling of density fluctuations $\rho \sim U_H^2 \rho_0 / g L_V$. Examining the present DNS results and previous experimental data, we confirmed that grid turbulence generated by a vertical grid behaves similarly to axisymmetric Saffman turbulence with $E(k) \sim k^2$ and time-independent $U_H^2 L_H^2 L_V$ and that the power laws derived for low-Re_b Saffman turbulence prevail when the Froude number Fr_M is sufficiently small. The main findings are summarized below.

The development of temporally evolving, stably stratified grid turbulence agrees well with the towed-grid experiments with similar Re_M and Fr_M (Praud *et al.* 2005). Before the grid turbulence has fully developed, there is a short time interval for which the rms velocity fluctuations stay almost constant for $Fr_M = 0.4$ and 1. This time interval expressed with the buoyancy period, tN, corresponds to the non-equilibrium regime (NEQ) of the wake that was found in a stably stratified turbulent wake of a sphere. Then, grid turbulence reaches a statistically homogeneous state and the velocity statistics become isotropic in the horizontal directions.

Temporally evolving grid turbulence results in the formation of homogeneous turbulence with $E(k) \sim k^2$ at a low-wavenumber range, which is the signature of Saffman turbulence. The auto-correlation functions have verified the partial self-similarity during the decay of stably stratified grid turbulence. The non-dimensional energy dissipation rate $\alpha = \varepsilon/(U_H^3/L_H)$ is approximately constant after $t/t_r \approx 20$ except for $Fr_M = 6$. However, α for $Fr_M = 6$ varies with time until $t/t_r \approx 100$. In each DNS, α hardly varies with time once grid turbulence has developed although it depends on Re_M and Fr_M. Our DNS results confirmed that $U_H^2 L_H^2 L_V$ hardly varies with time during the decay regardless of Re_M and Fr_M considered here. On the other hand, $U_H^2 L_H^4 L_V$ monotonically increases with time. The experimental data by Praud *et al.* (2005) was examined in this study and also showed that $U_H^2 L_H^2 L_V$ stays almost constant in their experiments. The time independence of $U_H^2 L_H^2 L_V$ suggested that the generated turbulence behaves similarly to axisymmetric Saffman turbulence. The temporal variations of U_H, L_H, L_V and ε for $Fr_M = 0.1\text{-}1$ exhibited power-law decays, whose exponents are close to the theoretical prediction for low-Re_b Saffman turbulence. We also evaluated the power-law exponents of U_H, L_H, L_V and ε with the experimental data at low Fr_M in Praud *et al.* (2005), and the exponents were also consistent with low-Re_b Saffman turbulence.

However, the decay of U_H^2 at $Fr_M = 6$ in the present DNS is not represented by a power law with a constant exponent and the decay rate depends on time because α is no longer constant for $t/t_r \lesssim 100$. Furthermore, the decay of U_H^2 after $t/t_r \gtrsim 100$ is still slower than the theoretical prediction. Previous experiments of stably stratified grid turbulence with $Fr_M = \mathcal{O}(10^0\text{-}10^1)$ have reported controversial results on the effects of stable stratification on the decay of horizontal velocity fluctuations. This is possibly explained by the temporal variation of the decay rate at moderately large Fr_M observed in the present DNS.

The decay of potential energy in the present DNS also follows the power law derived for low-Re_b Saffman turbulence when Fr_M is sufficiently small. Furthermore, the present DNS empirically suggested that the ratio between the potential and kinetic energy dissipation rates $\varepsilon_P/\varepsilon$ is proportional to Re_b when $Re_b \ll \mathcal{O}(10^0)$. This relation $\varepsilon_P/\varepsilon \sim Re_b$ was used to derive the decay law of ε_P of low-Re_b Saffman turbulence, which is also consistent with the DNS results at low Fr_M. The power-law decay of ε_P and ε for low-Re_b Saffman turbulence suggested that the mixing efficiency η_{mix} obeys a power law during the decay, where η_{mix} decreases with time. The behaviour of η_{mix} in the DNS is consistent with the theoretical prediction: $\eta_{mix} \approx 0.33$ weakly depends on time at the beginning of the decay while η_{mix} decreases as $\eta_{mix} \sim t^{-9/4}$ once Re_b becomes small.

Temporally evolving grid turbulence is initialized with a velocity field that approximates the mean velocity deficit of the wake of the grid. In the wavenumber space, this initial condition is represented by the energy spectrum with distinct peaks at wavenumbers related to the mesh size. Turbulence is generated by the turbulent production arising from mean shear while the effects of the grid object, such as vortex shedding, are ignored in the temporal model. Nonetheless, the temporally evolving grid turbulence exhibits the signatures of axisymmetric Saffman turbulence, such as $E(k) \sim k^2$ and invariance of $U_H^2 L_H^2 L_V$. We examined experimental data by Praud *et al.* (2005) and showed that a grid towed in a stably stratified fluid generates turbulence with constant $U_H^2 L_H^2 L_V$. These results suggest that the mean velocity deficit of the wakes is a key to the formation of axisymmetric Saffman turbulence in a stably stratified fluid.

Finally, it should be emphasized that the grid consisting of vertical plates was designed to avoid the excitation of strong internal waves (Fincham *et al.* 1996; Praud *et al.* 2005), which may have significant effects on turbulence generated by conventional square grids. Whether Saffman turbulence or Batchelor turbulence is generated depends on the generation process of turbulence. At least, experimental studies of non-stratified turbulence with square grids have reported that the decay properties are consistent with Saffman turbulence, e.g. constant $U^2 L^3$ during the decay (Krogstad & Davidson 2010; Kitamura *et al.* 2014). However, it is still possible that the wave excitation in a stably stratified fluid may affect the turbulence generation, and its influence on the decay of grid turbulence has to be addressed in future studies.

Direct numerical simulations presented in this paper were performed using the high-performance computing system in the Japan Agency for Marine-Earth Science and Technology. This work was also supported by "Collaborative Research Project on Computer Science with High-Performance Computing in Nagoya University" and by JSPS KAKENHI Grant Numbers 20H05754 and 22K03903.

Declaration of Interests

The authors report no conflict of interest

REFERENCES

Anas, M., Joshi, P. & Verma, M. K. 2020 Freely decaying turbulence in a finite domain at finite Reynolds number. *Phys. Fluids* **32** (9), 095109.

Antonia, R. A., Lee, S. K., Djenidi, L., Lavoie, P. & Danaila, L. 2013 Invariants for slightly heated decaying grid turbulence. *J. Fluid Mech.* **727**, 379–406.

Batchelor, G. K. 1953 *The Theory of Homogeneous Turbulence*. Cambridge Univ. Pr.

Batchelor, G. K. & Proudman, I. 1956 The large-scale structure of homogeneous turbulence. *Phil. Trans. R. Soc. A* **248**, 369–405.

Brethouwer, G., Billant, P., Lindborg, E. & Chomaz, J.-M. 2007 Scaling analysis and simulation of strongly stratified turbulent flows. *J. Fluid Mech.* **585**, 343–368.

Britter, R. E., Hunt, J. C. R., Marsh, G. L. & Snyder, W. H. 1983 The effects of stable stratification on turbulent diffusion and the decay of grid turbulence. *J. Fluid Mech.* **127**, 27–44.

de Bruyn Kops, S. M. & Riley, J. J. 2019 The effects of stable stratification on the decay of initially isotropic homogeneous turbulence. *J. Fluid Mech.* **860**, 787–821.

Chongsiripinyo, K. & Sarkar, S. 2020 Decay of turbulent wakes behind a disk in homogeneous and stratified fluids. *J. Fluid Mech.* **885**.

Comte-Bellot, G. & Corrsin, S. 1966 The use of a contraction to improve the isotropy of grid-generated turbulence. *J. Fluid Mech.* **25** (4), 657–682.

Davidson, P. A. 2004 *Turbulence: An Introduction for Scientists and Engineers*. Oxford Univ. Pr.

Davidson, P. A. 2009 The role of angular momentum conservation in homogeneous turbulence. *J. Fluid Mech.* **632**, 329–358.

Davidson, P. A. 2010 On the decay of Saffman turbulence subject to rotation, stratification or an imposed magnetic field. *J. Fluid Mech.* **663**, 268–292.

Davidson, P. A. 2013 *Turbulence in rotating, stratified and electrically conducting fluids*. Cambridge University Press.

Diamessis, P. J., Spedding, G. R. & Domaradzki, J. A. 2011 Similarity scaling and vorticity structure in high-Reynolds-number stably stratified turbulent wakes. *J. Fluid Mech.* **671**, 52–95.

Djenidi, L., Kamruzzaman, Md. & Antonia, R. A. 2015 Power-law exponent in the transition period of decay in grid turbulence. *J. Fluid Mech.* **779**, 544–555.

Espa, S., Avallone, G. & Cenedese, A. 2018 Decaying grid turbulence experiments in a stratified fluid: flow measurements and statistics. *Stoch. Environ. Res. Risk Assess.* **32** (8), 2325–2336.

Fincham, A. M., Maxworthy, T. & Spedding, G. R. 1996 Energy dissipation and vortex structure in freely decaying, stratified grid turbulence. *Dyn. Atmos. Oceans* **23** (1-4), 155–169.

Gampert, M., Boschung, J., Hennig, F., Gauding, M. & Peters, N. 2014 The vorticity versus the scalar criterion for the detection of the turbulent/non-turbulent interface. *J. Fluid Mech.* **750**, 578–596.

Godoy-Diana, R., Chomaz, J.-M. & Billant, P. 2004 Vertical length scale selection for pancake vortices in strongly stratified viscous fluids. *J. Fluid Mech.* **504**, 229–238.

Goto, S & Vassilicos, J. C. 2016 Unsteady turbulence cascades. *Phys. Rev. E* **94** (5), 053108.

Gregg, M. C., D'Asaro, E. A., Riley, J. J. & Kunze, E. 2018 Mixing efficiency in the ocean. *Annu. Rev. Mar. Sci.* **10**, 443–473.

Hayashi, M., Watanabe, T. & Nagata, K. 2021 Characteristics of small-scale shear layers in a temporally evolving turbulent planar jet. *J. Fluid Mech.* **920**, A38.

Huq, P. & Britter, R. E. 1995 Turbulence evolution and mixing in a two-layer stably stratified fluid. *J. Fluid Mech.* **285**, 41–67.

Isaza, J. C., Salazar, R. & Warhaft, Z. 2014 On grid-generated turbulence in the near-and far field regions. *J. Fluid Mech.* **753**, 402–426.

Ishida, T., Davidson, P. A. & Kaneda, Y. 2006 On the decay of isotropic turbulence. *J. Fluid Mech.* **564**, 455–475.

Ishihara, T., Gotoh, T. & Kaneda, Y. 2009 Study of high–Reynolds number isotropic turbulence by direct numerical simulation. *Annu. Rev. Fluid Mech.* **41**, 165–180.

Itsweire, E. C., Helland, K. N. & Van Atta, C. W. 1986 The evolution of grid-generated turbulence in a stably stratified fluid. *J. Fluid Mech.* **162**, 299–338.

Kitamura, T., Nagata, K., Sakai, Y., Sasoh, A., Terashima, O., Saito, H. & Harasaki, T. 2014 On invariants in grid turbulence at moderate Reynolds numbers. *J. Fluid Mech.* **738**, 378–406.

Komori, S. & Nagata, K. 1996 Effects of molecular diffusivities on counter-gradient scalar and momentum transfer in strongly stable stratification. *J. Fluid Mech.* **326**, 205–237.

Komori, S., Nagata, K., Kanzaki, T. & Murakami, Y. 1993 Measurements of mass flux in a turbulent liquid flow with a chemical reaction. *AIChE J.* **39** (10), 1611–1620.

Kozul, M., Chung, D. & Monty, J. P. 2016 Direct numerical simulation of the incompressible temporally developing turbulent boundary layer. *J. Fluid Mech.* **796**, 437–472.

Krogstad, P.-Å. & Davidson, P. A. 2010 Is grid turbulence Saffman turbulence? *J. Fluid Mech.* **642**, 373–394.

Krogstad, P.-Å. & Davidson, P. A. 2012 Near-field investigation of turbulence produced by multi-scale grids. *Phys. Fluids* **24** (3), 035103.

Lavoie, P., Djenidi, L. & Antonia, R. A. 2007 Effects of initial conditions in decaying turbulence generated by passive grids. *J. Fluid Mech.* **585**, 395–420.

Lienhard, J. H. & van Atta, C. W. 1990 The decay of turbulence in thermally stratified flow. *J. Fluid Mech.* **210**, 57–112.

Lindborg, E. 2006 The energy cascade in a strongly stratified fluid. *J. Fluid Mech.* **550**, 207–242.

Liu, H.-T. 1995 Energetics of grid turbulence in a stably stratified fluid. *J. Fluid Mech.* **296**, 127–157.

Maffioli, A., Brethouwer, G. & Lindborg, E. 2016 Mixing efficiency in stratified turbulence. *J. Fluid Mech.* **794**.

Maffioli, A. & Davidson, P. A. 2016 Dynamics of stratified turbulence decaying from a high buoyancy Reynolds number. *J. Fluid Mech.* **786**, 210–233.

Mahrt, L. 1999 Stratified atmospheric boundary layers. *Boundary-Layer Meteorol.* **90** (3), 375–396.

Mazellier, N. & Vassilicos, J. C. 2008 The turbulence dissipation constant is not universal because of its universal dependence on large-scale flow topology. *Phys. Fluids* **20** (1), 015101.

Melina, G., Bruce, P. J. K. & Vassilicos, J. C. 2016 Vortex shedding effects in grid-generated turbulence. *Phys. Rev. Fluids* **1** (4), 044402.

Mohamed, M. S. & LaRue, J. C. 1990 The decay power law in grid-generated turbulence. *J. Fluid Mech.* **219**, 195–214.

Mora, D. O., Pladellorens, E. M., Turró, P. R., Lagauzere, M. & Obligado, M. 2019 Energy cascades in active-grid-generated turbulent flows. *Phys. Rev. Fluids* **4** (10), 104601.

Morinishi, Y., Lund, T. S., Vasilyev, O. V. & Moin, P. 1998 Fully conservative higher order finite difference schemes for incompressible flow. *J. Comput. Phys.* **143** (1), 90–124.

Nagata, K., Saiki, T., Sakai, Y., Ito, Y. & Iwano, K. 2017 Effects of grid geometry on non-equilibrium dissipation in grid turbulence. *Phys. Fluids* **29** (1), 015102.

Nagata, K., Sakai, Y., Inaba, T., Suzuki, H., Terashima, O. & Suzuki, H. 2013 Turbulence structure and turbulence kinetic energy transport in multiscale/fractal-generated turbulence. *Phys. Fluids* **25** (6), 065102.

Okino, S. & Hanazaki, H. 2019 Decaying turbulence in a stratified fluid of high Prandtl number. *J. Fluid Mech.* **874**, 821–855.

Panchapakesan, N. R.and Lumley, J. L. 1993 Turbulence measurements in axisymmetric jets of air and helium. Part 1. Air jet. *J. Fluid Mech.* **246**, 197–223.

Pham, H. T., Sarkar, S. & Brucker, K. A. 2009 Dynamics of a stratified shear layer above a region of uniform stratification. *J. Fluid Mech.* **630**, 191–223.

Pope, S. B. 2000 *Turbulent Flows*. Cambridge Univ. Pr.

Praud, O., Fincham, A. M. & Sommeria, J. 2005 Decaying grid turbulence in a strongly stratified fluid. *J. Fluid Mech.* **522**, 1–33.

Rehmann, C. R. & Koseff, J. R. 2004 Mean potential energy change in stratified grid turbulence. *Dyn. Atmos. Oceans* **37** (4), 271–294.

Riley, J. J. & de Bruyn Kops, S. M. 2003 Dynamics of turbulence strongly influenced by buoyancy. *Phys. Fluids* **15** (7), 2047–2059.

Saffman, P. G. 1967 The large-scale structure of homogeneous turbulence. *J. Fluid Mech.* **27**, 581–593.

Salehipour, H, Peltier, WR & Mashayek, A 2015 Turbulent diapycnal mixing in stratified shear flows: the influence of Prandtl number on mixing efficiency and transition at high Reynolds number. *J. Fluid Mech.* **773**, 178–223.

Sarpkaya, T. 2006 Structures of separation on a circular cylinder in periodic flow. *J. Fluid Mech.* **567**, 281–297.

Seoud, R. E. & Vassilicos, J. C. 2007 Dissipation and decay of fractal-generated turbulence. *Phys. Fluids* **19** (10), 105108.

da Silva, C. B. & Pereira, J. C. F. 2008 Invariants of the velocity-gradient, rate-of-strain, and rate-of-rotation tensors across the turbulent/nonturbulent interface in jets. *Phys. Fluids* **20** (5), 055101.

Simmonsr, L. F. G. & Salter, C. 1934 Experimental investigation and analysis of the velocity variations in turbulent flow. *Proc. R. Soc. Lond. A* **145** (854), 212–234.

Sinhuber, M., Bodenschatz, E. & Bewley, G. P. 2015 Decay of turbulence at high Reynolds numbers. *Phys. Rev. Lett.* **114** (3), 034501.

Smyth, W. D., Moum, J. N. & Caldwell, D. R. 2001 The efficiency of mixing in turbulent patches: Inferences from direct simulations and microstructure observations. *J. Phys. Oceanogr.* **31** (8), 1969–1992.

Spedding, G. R. 1997 The evolution of initially turbulent bluff-body wakes at high internal Froude number. *J. Fluid Mech.* **337**, 283–301.

Stillinger, D. C., Helland, K. N. & Van Atta, C. W. 1983 Experiments on the transition of homogeneous turbulence to internal waves in a stratified fluid. *J. Fluid Mech.* **131**, 91–122.

Takamure, K., Sakai, Y., Ito, Y., Iwano, K. & Hayase, T. 2019 Dissipation scaling in the transition region of turbulent mixing layer. *Int. J. Heat Fluid Flow* **75**, 77–85.

Taveira, R. R. & da Silva, C. B. 2013 Kinetic energy budgets near the turbulent/nonturbulent interface in jets. *Phys. Fluids* **25**, 015114.

Teitelbaum, T. & Mininni, P. D. 2012 Decay of Batchelor and Saffman rotating turbulence. *Phys. Rev. E* **86** (6), 066320.

Thorpe, S. A. 1978 The near-surface ocean mixing layer in stable heating conditions. *J. Geophys. Res.* **83** (C6), 2875–2885.

Uberoi, M. S. & Wallis, S. 1967 Effect of grid geometry on turbulence decay. *Phys. Fluids* **10**, 1216–1224.

Valente, P. C., da Silva, C. B. & Pinho, F. T. 2016 Energy spectra in elasto-inertial turbulence. *Phys. Fluids* **28** (7), 075108.

Valente, P. C. & Vassilicos, J. C. 2011 The decay of turbulence generated by a class of multiscale grids. *J. Fluid Mech.* **687**, 300–340.

Valente, P. C. & Vassilicos, J. C. 2015 The energy cascade in grid-generated non-equilibrium decaying turbulence. *Phys. Fluids* **27** (4), 045103.

VanDine, A., Pham, H. T. & Sarkar, S. 2021 Turbulent shear layers in a uniformly stratified background: DNS at high Reynolds number. *J. Fluid Mech.* **916**.

Vassilicos, J. C. 2015 Dissipation in turbulent flows. *Annu. Rev. Fluid Mech.* **47**, 95–114.

Watanabe, T. & Nagata, K. 2018 Integral invariants and decay of temporally developing grid turbulence. *Phys. Fluids* **30** (10), 105111.

Watanabe, Tomoaki & Nagata, Koji 2021 Large-scale characteristics of a stably stratified turbulent shear layer. *J. Fluid Mech.* **927**, A27.

Watanabe, T., Riley, J. J., Nagata, K., Matsuda, K. & Onishi, R. 2019*a* Hairpin vortices and highly elongated flow structures in a stably stratified shear layer. *J. Fluid Mech.* **878**, 37–61.

Watanabe, T., Riley, J. J., Nagata, K., Onishi, R. & Matsuda, K. 2018*a* A localized

turbulent mixing layer in a uniformly stratified environment. *J. Fluid Mech.* **849**, 245–276.

Watanabe, T., Sakai, Y., Nagata, K. & Ito, Y. 2016 Large eddy simulation study of turbulent kinetic energy and scalar variance budgets and turbulent/non-turbulent interface in planar jets. *Fluid Dyn. Res.* **48** (2), 021407.

Watanabe, T., Sakai, Y., Nagata, K., Ito, Y. & Hayase, T. 2015 Turbulent mixing of passive scalar near turbulent and non-turbulent interface in mixing layers. *Phys. Fluids* **27** (8), 085109.

Watanabe, T., Tanaka, K. & Nagata, K. 2020 Characteristics of shearing motions in incompressible isotropic turbulence. *Phys. Rev. Fluids* **5** (7), 072601.

Watanabe, T., Zhang, X. & Nagata, K. 2018*b* Turbulent/non-turbulent interfaces detected in DNS of incompressible turbulent boundary layers. *Phys. Fluids* **30** (3), 035102.

Watanabe, T., Zhang, X. & Nagata, K. 2019*b* Direct numerical simulation of incompressible turbulent boundary layers and planar jets at high Reynolds numbers initialized with implicit large eddy simulation. *Comput. Fluids* **194**, 104314.

Yap, C. T. & Van Atta, C. W. 1993 Experimental studies of the development of quasi-two-dimensional turbulence in stably stratified fluid. *Dyn. Atmos. Oceans* **19** (1-4), 289–323.

Yoon, K. & Warhaft, Z. 1990 The evolution of grid-generated turbulence under conditions of stable thermal stratification. *J. Fluid Mech.* **215**, 601–638.

Yoshimatsu, K. & Kaneda, Y. 2018 Large-scale structure of velocity and passive scalar fields in freely decaying homogeneous anisotropic turbulence. *Phys. Rev. Fluids* **3** (10), 104601.

Zecchetto, M. & da Silva, C. B. 2021 Universality of small-scale motions within the turbulent/non-turbulent interface layer. *J. Fluid Mech.* **916**.

Zheng, Y., Nagata, K. & Watanabe, T. 2021*a* Energy dissipation and enstrophy production/destruction at very low Reynolds numbers in the final stage of the transition period of decay in grid turbulence. *Phys. Fluids* **33** (3), 035147.

Zheng, Y., Nagata, K. & Watanabe, T. 2021*b* Turbulent characteristics and energy transfer in the far field of active-grid turbulence. *Phys. Fluids* **33** (11), 115119.

Zhou, Q. & Diamessis, P. J. 2019 Large-scale characteristics of stratified wake turbulence at varying Reynolds number. *Phys. Rev. Fluids* **4** (8), 084802.